Applied Ocean Research 50 (2015) 69–90

Contents lists available at ScienceDirect

Applied Ocean Research

journal homepage: www.elsevier.com/locate/apor

Rankine time-domain method with application to side-by-side gap flow modeling

R.A. Watai [a,*], P. Dinoi [b], F. Ruggeri [a], A. Souto-Iglesias [b], A.N. Simos [a]

[a] Numerical Offshore Tank (TPN), Department of Naval Architecture and Ocean Engineering – University of Sao Paulo, Sao Paulo, SP, Brazil
[b] Naval Architecture Department, Technical University of Madrid, Madrid, Spain

ARTICLE INFO

Article history:
Received 21 July 2014
Received in revised form 23 October 2014
Accepted 9 December 2014
Available online 30 January 2015

Keywords:
Time domain Rankine panel method
Gap resonant effects
Multibody hydrodynamic interaction
Damping lid technique
Side-by-side

ABSTRACT

The performance of a time domain Rankine panel method applied to the seakeeping problem of two ships in side-by-side configuration is investigated in this article. Benchmark data for the numerical results are provided by fundamental seakeeping tests carried out in the towing tank of the CEHINAV-Technical University of Madrid. The multi-body system was composed by a barge and a prismatic geosim, which were subjected to regular head waves in two different gap distances. The motions of the geosim model were restricted to surge, heave and pitch, whereas the barge model was kept fixed. This set-up was adopted so as to guarantee that the gap width remained constant during the tests, providing a favorable situation for the numerical modeling of the system. Comparison between measurements and numerical results illustrates the limitation of potential flow solvers concerning the modeling of this hydrodynamic problem. Numerical wave resonance in the gap led to wave elevations and body motions much larger than those observed during the tests. In addition, the time domain method also presented convergence problems for a range of frequencies associated to the gap resonance phenomenon. In order to overcome these problems, an external damping factor was introduced in the time domain simulations, bringing a significant improvement to the numerical convergence of the method. Moreover, despite the simplicity of the damping model adopted, the results showed that this technique was indeed able to improve the computational predictions, leading to a closer agreement between the experiments and the numerical results.

1. Introduction

The hydrodynamic interaction of two vessels in a side-by-side arrangement is currently receiving substantial attention due to its practical application in the offloading process involving the so-called FLNG (Floating Liquefied Natural Gas) units and LNG (Liquefied Natural Gas) carriers. As a result, much attention has been given to the analysis of multi-body interaction effects with regard to the prediction of risk of collision between the vessels [1]. In this regard, the correct modeling of the fully coupled dynamics of this multi-body problem and also the prediction of the vessels relative motions are important aspects when planning of such a complex operation [2]. Indeed, this analysis must also be taken into account in the design of a mooring system for this kind of operation [3].

Wave resonant effects in the gap is one of the challenging problems in the hydrodynamic modeling of two bodies arranged in a side-by-side configuration. These resonances create different mode shapes of wave elevation in the gap at each associated resonant frequency, which is a behavior quite similar to the one that takes place in moonpools [4]. The three basic modes are normally referred to as the piston mode, longitudinal and transversal sloshing. An approximation formula for the estimation of these frequencies in open boundaries may be found in [5]. A comprehensive numerical investigation with the purpose of studying the different resonant frequencies and modes is given by Sun et al. [6].

Occurrence of gap wave resonant effects in problems involving bodies arranged in side-by-side has already been observed by several authors (see for instance [7–9]). Although, in reality, resonant effects in the wave height may occur in the gap, they are largely dampened by viscous effects and, therefore, the conventional potential flow methods are known to over-estimate the hydrodynamic forces, the wave elevation in the gap and consequently the body motions. This occurs because these methods are unable to model the viscous effects, namely skin friction and flow separation on the hull side, that are deemed important, especially the latter, for the flow in the small gap between the hulls [10,11].

CFD applications for dealing with the viscous effects in this resonant problem are certainly envisaged, but, to this moment, the high computational effort they demand still renders these applications infeasible for practical engineering purposes. For this

* Corresponding author. Tel.: +55 11 34414505.
E-mail addresses: rafawatai@gmail.com, rafael.watai@usp.br (R.A. Watai).

0141-1187/$ – see front matter © 2014 Elsevier Ltd. All rights reserved.
http://dx.doi.org/10.1016/j.apor.2014.12.002

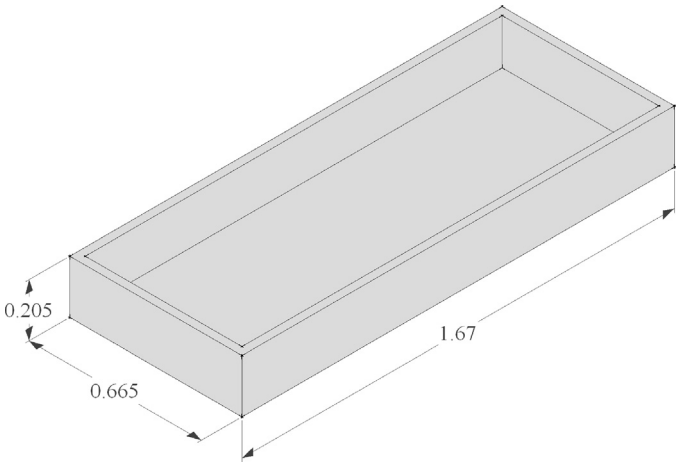

Fig. 1. Barge geometry and main dimensions in meters.

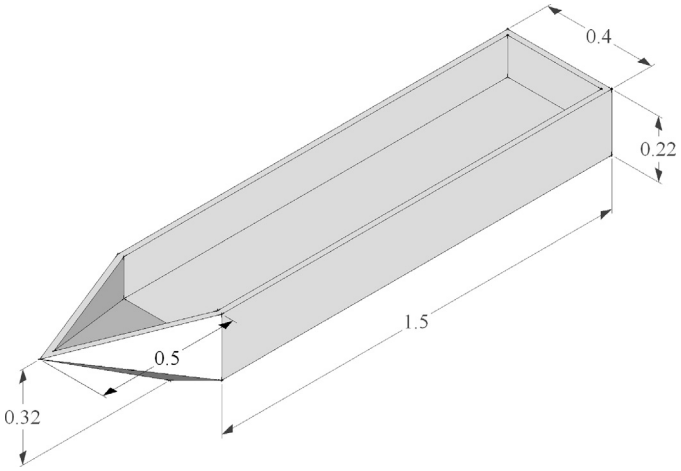

Fig. 2. Geosim geometry and main dimensions in meters.

reason, mixed approaches combining the benefits provided by viscous and potential flow solvers may be considered as a promising alternative to handle the problem. Kristiansen and Faltinsen [12] applied this methodology in a two-dimensional numerical wave tank with a floating body. Elie et al. [13] presented numerical results computed with their three-dimensional SWENSE (Spectral Wave

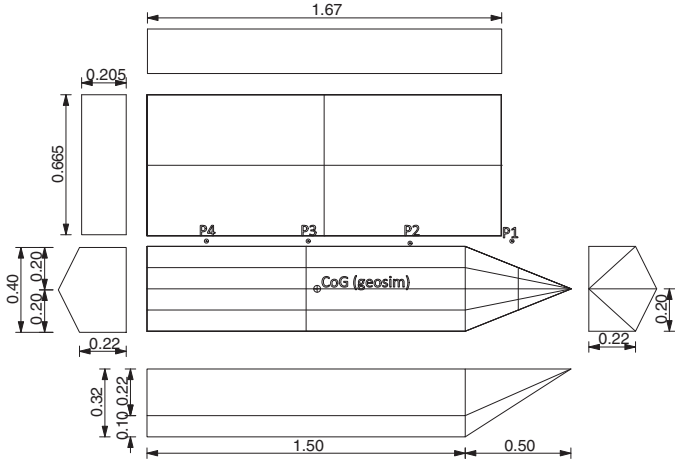

Fig. 3. Details of the geosim geometry and main dimensions in meters.

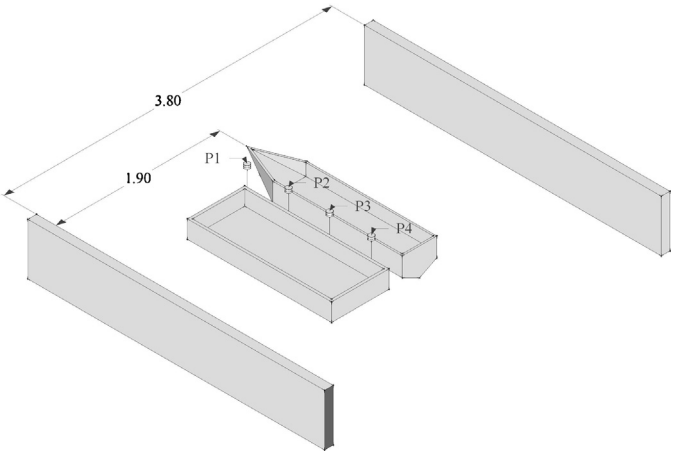

Fig. 4. Models positions in relation to the towing tank walls. Dimensions in meters.

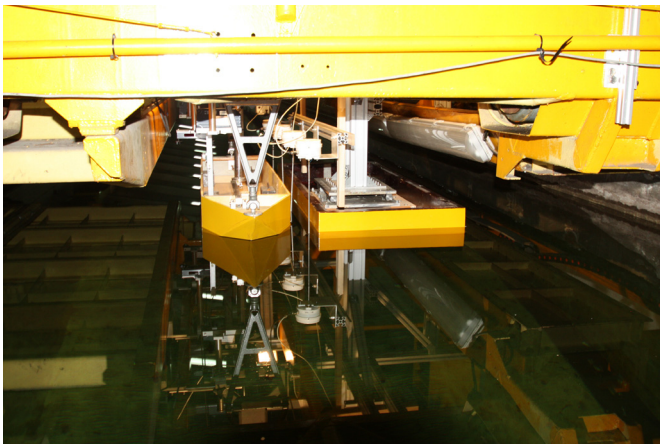

Fig. 5. General view of the models positioned in the tank.

Explicit Navier–Stokes Equations) numerical method for two side-by-side fixed barges in different regular waves incident angles.

However, for the time being, computational methods most often applied to model the side-by-side problem are based on the potential flow theory, in which suppression methods to deal with the resonant problems are used as an attempt to better reproduce the physics of the phenomenon. In the context of linear frequency domain diffraction/radiation codes, Huijsmans et al. [7] imposed a no flux vertical condition by applying a rigid lid along the gap

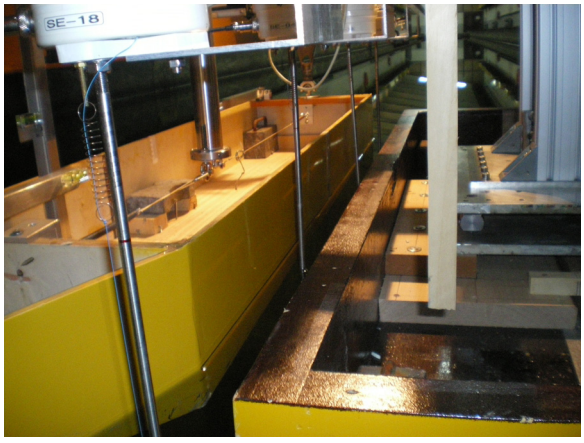

Fig. 6. Wave probes arranged along the gap centerline.

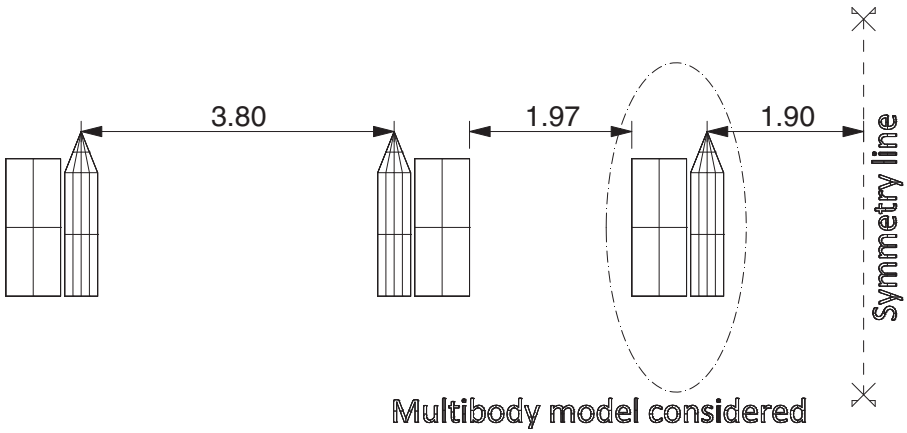

Fig. 7. Symmetries applied for the multi-body model. Dimensions in meters.

length. Newman [14] improved the lid method using the generalized mode technique with a set of basis functions composed of Chebyshev polynomials. This method allows wave motion in the gap, in which the wave elevation is controlled by imposing damping factors for each generalized mode.

In a different approach, Chen [15] formulated a suppression method, namely the damping lid method, introducing a damping force directly into the conventional free surface boundary conditions. A major advantage of this method is that only one value of damping factor is needed. A first attempt for applying this method is presented in Fournier et al. [16], where comparisons between numerical and experimental results, for a FSRU (Floating Storage and Regasification Unit) and a LNG carrier positioned in side-by-side, attested that the method was effective in attenuating the wave elevation in the confined zone, which consequently led to a better reproduction of the first order motions and drift forces. Following the same approach, Pauw et al. [17] applied the damping lid method for the investigation of resonant effects considering LNG carriers in side-by-side. Experimental tests were conducted considering only one ship model, which was positioned at half-gap width from the lateral tank wall. Results were discussed in terms of wave elevation in the gap, motion RAOs (Response Amplitude Operators) and wave drift QTFs (Quadratic Transfer Functions). The authors concluded that the damping factor has a much greater effect on the drift forces than on the first order quantities and that an unique value of damping parameter was not enough to provide a full agreement with the test data. Furthermore, a slight frequency shift in wave elevations and vessels motions between measurements and

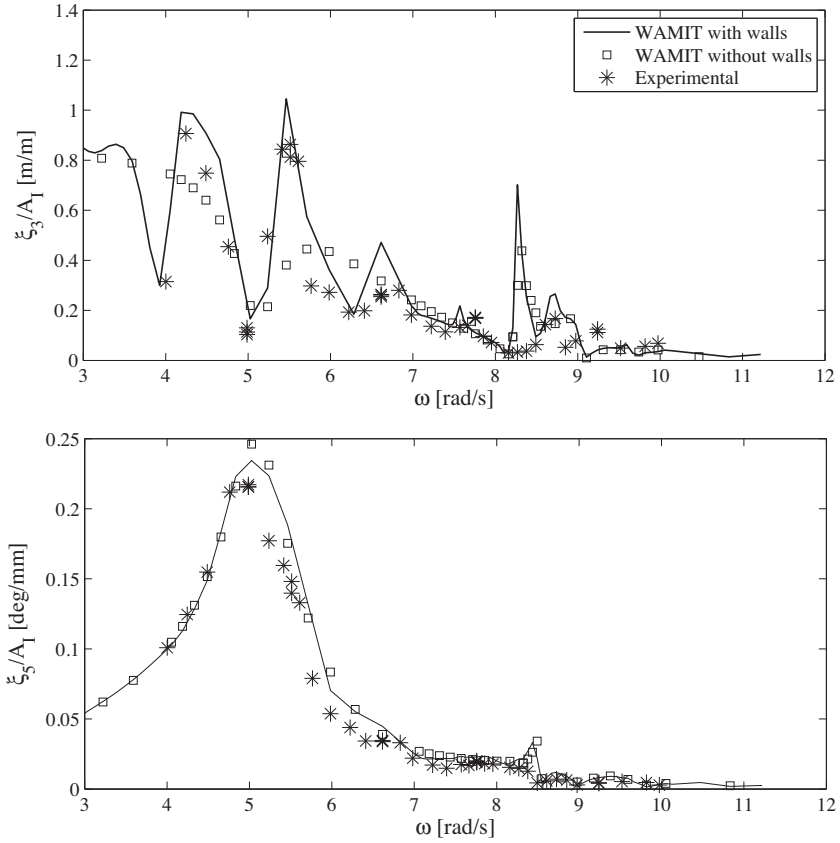

Fig. 8. Case 1: Comparison between WAMIT numerical data and experimental values in terms of heave (top) and pitch (bottom) RAOs. Gap width = 0.05 m.

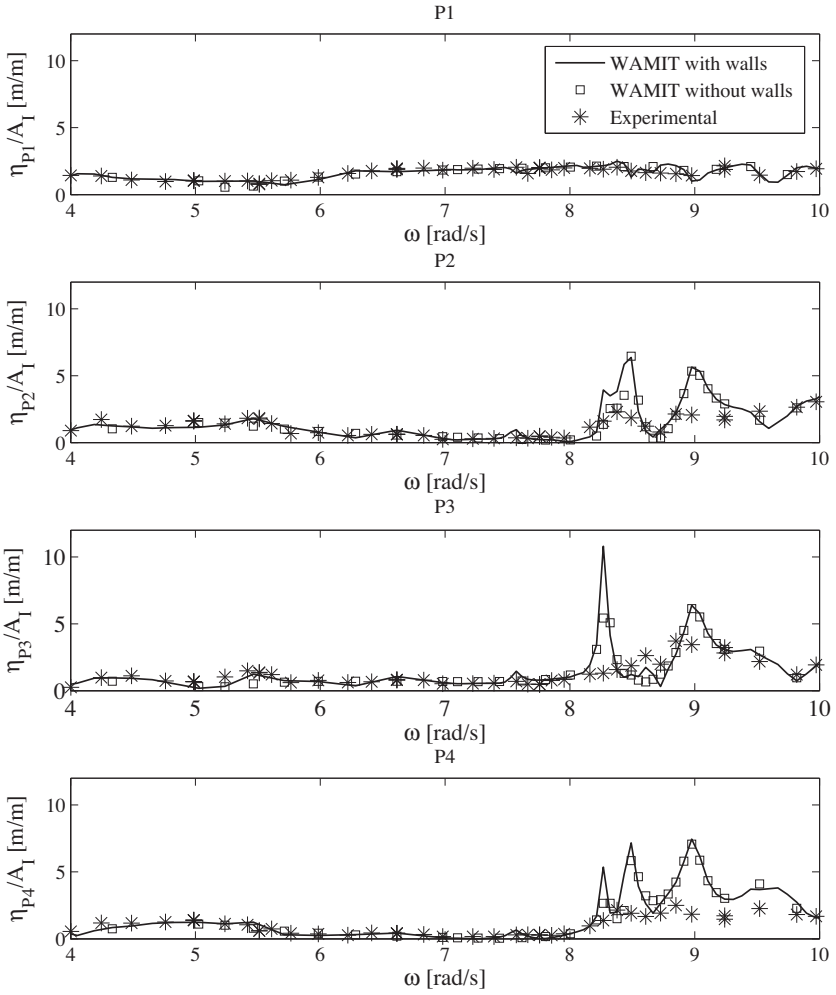

Fig. 9. Case 1: Comparison between WAMIT numerical data and experimental values in terms of wave elevations RAOs in different points positioned along the gap centerline. Gap width = 0.05 m.

diffraction results was observed. Bunnik et al. [18] overcame this inconsistent frequency shift problem by applying the damping lid technique not only in the gap but also inside the hulls, in order to remove the so-called irregular frequencies (those generated by the spurious numerical solution of internal problems inside the hulls). In fact, the authors have shown that such inconsistency of the numerical scheme was related to the rigid lid imposed inside the bodies to remove the irregular frequencies of the solution, which was introducing a strong grid dependence into the computations.

Hong et al. [19] presented a study comparing the performance of a discontinuous HOBEM with a wetted surface damping condition and a constant BEM combined with a damped free surface condition on predicting first-order solutions and repulsive drift forces of two identical caissons in side-by-side. Results showed that both methods were effective for damping the first-order quantities associated to the first gap resonant frequency. Concerning the second-order drift forces, a better prediction of available experimental data was achieved by using the HOBEM with a tuned wetted surface damping parameter.

Clauss et al. [20] compared numerical and experimental results considering a barge-LNG carrier system and found numerical resonance peaks in the heave RAO, but not in the wave elevation inside the gap. In contrast with the majority of the previous works, they concluded that no external damping was necessary for modeling the wave elevations observed in the gap. This sort of discrepancy found among recent works on the theme emphasizes that additional systematic studies are still needed for a more comprehensive understanding of the flow phenomena and the performance of the computational techniques available for modeling them.

The analysis of multi-body hydrodynamic interactions have also being studied in time domain [21,2,22,23]. This approach is often used when the fully-coupled analysis involving not only the bodies, but also the mooring lines and fenders must be assessed, a situation in which a time domain approach must be necessarily applied. All these works, however, were based on the use of Cummins's equations [24], in which frequency domain hydrodynamic coefficients are used as input data for the time domain calculations.

An alternative approach is to treat the hydrodynamic problem directly in time domain. Kim and Kim [25] applied a time domain boundary elements method for studying the motion responses of adjacent vessels. They reproduced the resonant modes but did not make any attempt to suppress the resonant effects. Although the authors presented only linear results, the method can be extended to nonlinear problems by considering the nonlinear restoring and Froude–Krylov forces. Applications of time domain codes to side-by-side problems, including nonlinear results, were also presented by Yan et al. [26] and Hong and Nam [27]. In the latter, a poor convergence on the time series of the second order sway forces was observed for resonant frequencies. These studies were based on the finite element method technique and also disregarded any sort of artificial damping in the gap.

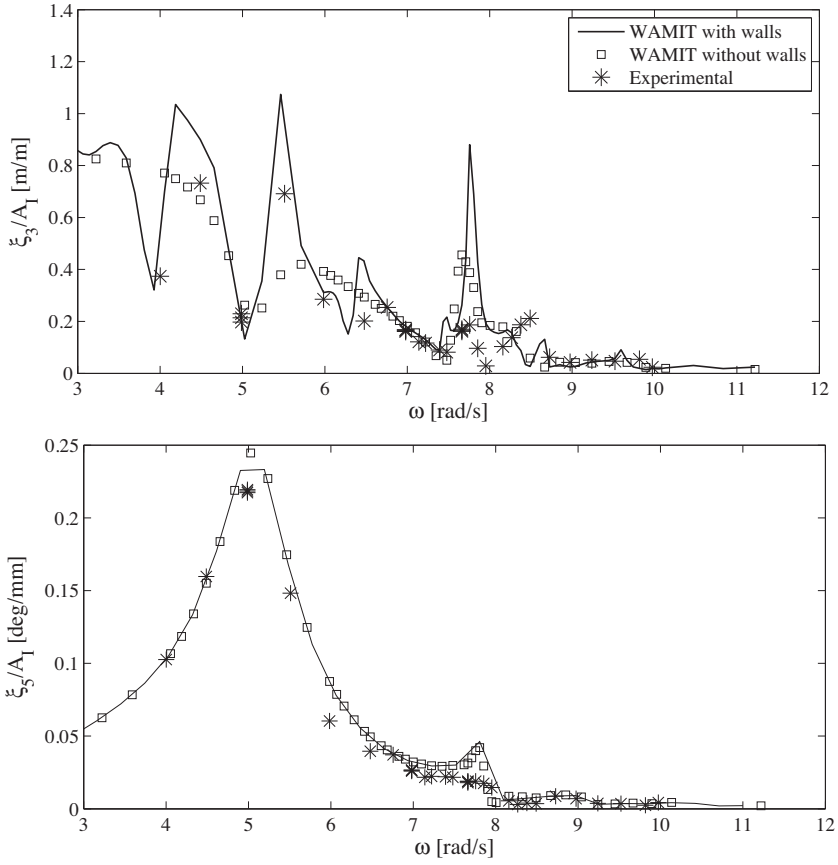

Fig. 10. Case 2: Comparison between WAMIT numerical data and experimental values in terms of heave (top) and pitch (below) RAOs. Gap width = 0.1 m.

Although the number of studies related to the application of time domain hydrodynamic solvers is still small in comparison to the conventional frequency domain method, it does represent a promising approach for the seakeeping analysis of fully coupled multi-body systems comprised by floating bodies, mooring lines, fenders etc. Nevertheless, the performance of suppression methods modeled in time domain potential flow solvers is a topic that still requires further investigation.

With this in mind, this paper discusses the performance of a time domain Rankine panel method (TDRPM) applied to a multi-body system in side-by-side configuration. Currently, TDRPM neglects the nonlinear effects originated from the presence of unknown free surface and body surface positions [28]. TDRPM is being developed in the context of a research project that aims at coupling the time domain hydrodynamic solver to the dynamic simulator of the Numerical Offshore Tank of the University of Sao Paulo (TPN-USP), which also takes into account the effects of wind, current, mooring lines and risers. Nowadays, the TPN software is based on Cummins's equations and considers, as input data, a set of linear hydrodynamic coefficients (added mass, potential damping, exciting and drift forces, etc.) previously computed by the frequency domain software WAMIT [29]. One of the main issues of this approach emerges from problems involving more than one body, in which the transient hydrodynamic interaction that results from large relative displacements of the bodies must be taken into account. The offloading operation of an Floating Production Storage and Offloading (FPSO) unit is an example of this type of problem, in which, due to the proximity of the FPSO and the shuttle tanker, the wave effects induced by the vessels have an important role in the hydrodynamic loads and, consequently, in the dynamics of such a complex operation ([30,31]). In this sense, a first benefit of incorporating a time domain hydrodynamic solver into the TPN software would be the possibility to handle these multi-body transient problems more properly in the future, even when applying, in a first moment, a linear method. In addition, in comparison to models mathematically treated in frequency domain, this approach also allows addressing future extensions to nonlinear descriptions of the hydrodynamic problem in a more straightforward manner. In this regard, extensions of the code to deal with nonlinear and wave–current interaction problems are already under development.

For the present side-by-side problem, fundamental tests with simplified geometries were carried out at the model basin of CEHINAV-Technical University of Madrid (UPM) in order to provide benchmark data for the TDRPM numerical simulations. Moreover, the results were also compared to the ones calculated by the software WAMIT, which was also used for the conceptual planning of the experiments.

As expected, results show that the numerical methods indeed tend to overestimate the experimental data for the natural resonant frequencies of the two gaps tested. As will be presented, these gap resonant frequencies cause problems of convergence in the method, which were also observed in the computations performed by Hong and Nam [27]. In order to eliminate this problem, the damping lid method was applied in the time-domain TDRPM and the convergence of the time series with different damping levels was investigated. To the authors knowledge, this is the first time that certain issues concerning the numerical modeling of the resonant effects in time-domain are reported in the literature specialized in side-by-side operations. Furthermore, the results also point out that the damping lid method improves the reproduction of the experimental data, which may be considered as a positive

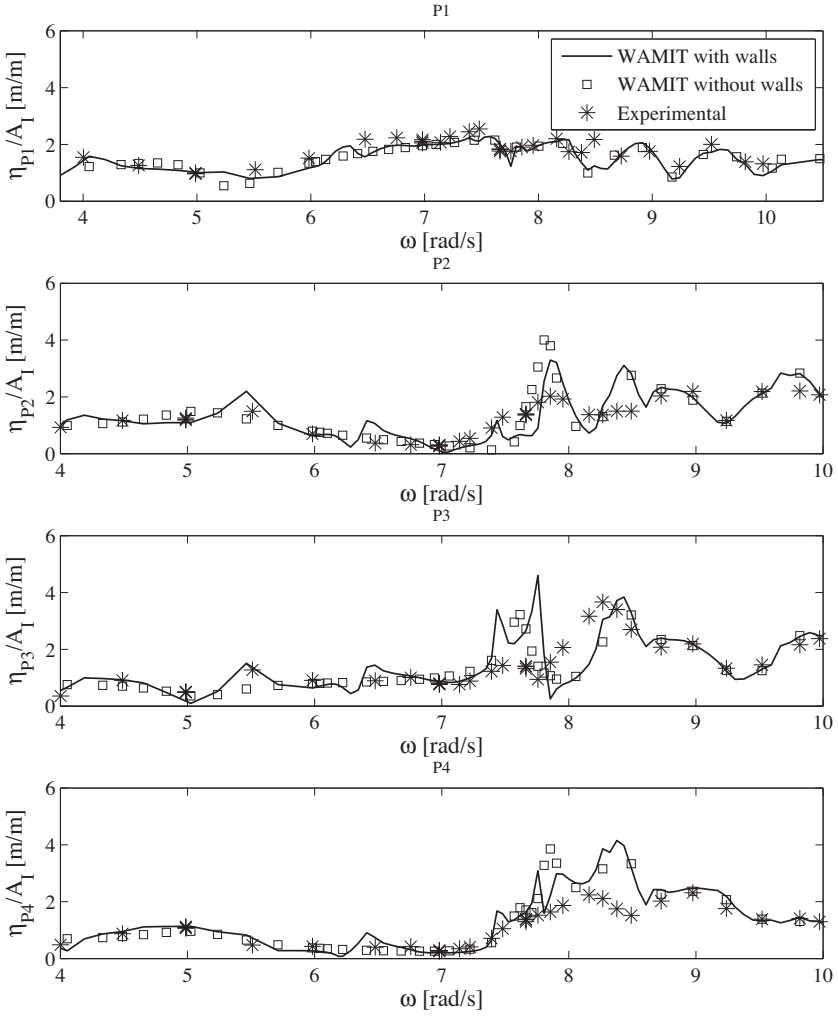

Fig. 11. Case 2: Comparison between WAMIT numerical data and experimental values in terms of wave elevations RAOs in different points positioned along the gap centerline. Gap width = 0.1 m.

indication for future simulations involving irregular waves. Indeed, preventing numerical convergence problems along the computations is a critical issue for simulating irregular wave conditions in time domain. This was the main goal for investigating the performance of the damping lid technique, even though the limitations of the simplified approach adopted herein are obvious. One must bear in mind that not only the physics of the flow is not captured by this sort of technique, but also that the damping factors that will be adopted to emulate this physics are considered constant in this work, irrespective of the wave amplitudes and frequencies. It is important to emphasize that, despite of the simplicity of the flow model adopted, the numerical method was in fact able to reproduce closely the trends observed in the resonant responses for most of the cases, as the results ahead will show.

The presents article is organized as follows: In Section 2, case studies geometries, main particulars, configurations and test matrix are described; in Section 3, the numerical methods used are presented. Numerical and experimental results of motion and gap wave heights are discussed in Section 4. Finally, Section 5 presents the main conclusions and future works threads.

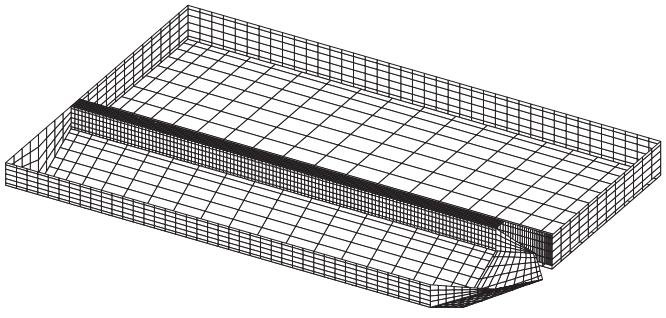

Fig. 12. Barge, geosim and gap panel meshes for Case 1.

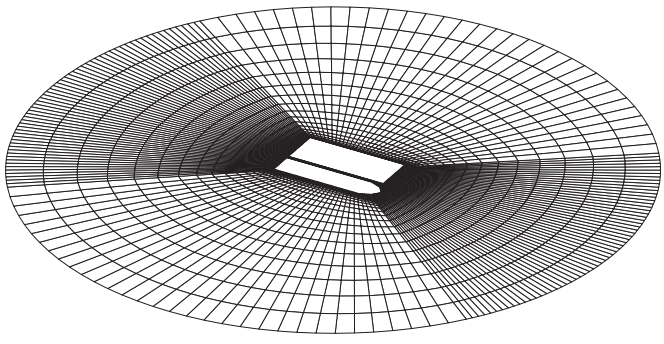

Fig. 13. Free surface panel mesh for Case 1.

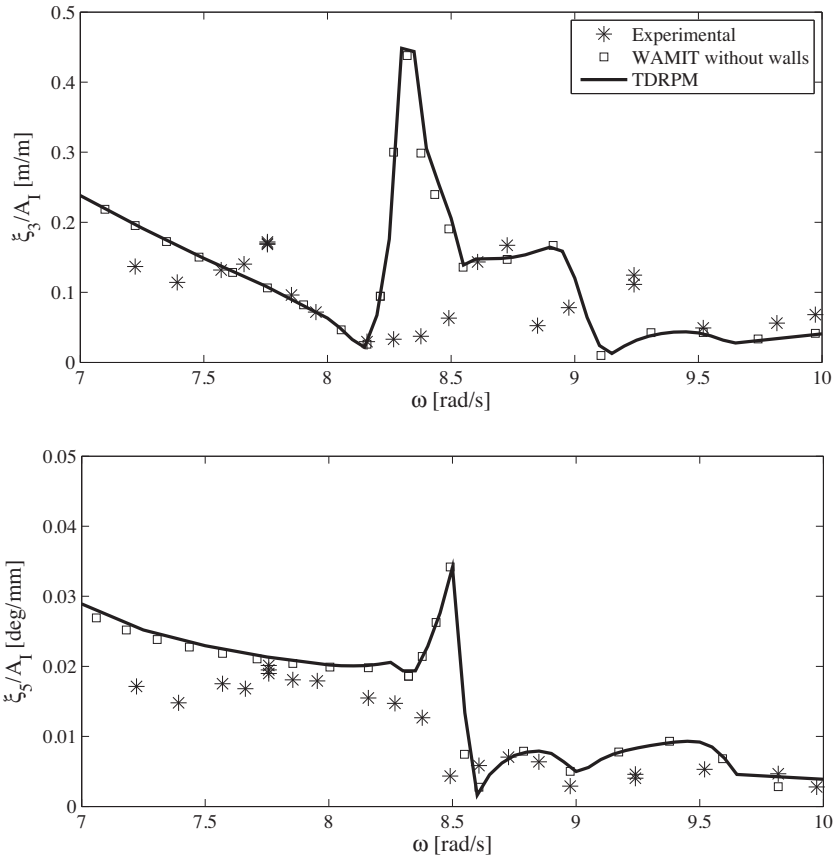

Fig. 14. Case 1: Comparison between WAMIT, TDRPM and experimental values in terms of heave (top) and pitch (bottom) RAOs. Gap width = 0.05 m.

2. Experimental setup

The experimental tests considered a multibody system comprising two bodies of canonical geometries, namely a barge and a geosim, arranged in two different side-by-side configurations. The main characteristics of the models are presented in Table 1 and illustrated in Figs. 1–3, the latter presenting the geosim geometry in detail. The tests were conducted at the towing tank of the CEHINAV-Technical University of Madrid (UPM). The tank is 100 m long, 3.8 m wide and the water depth is 2.5 m.

The tests were restricted to very simple configurations, aiming at providing benchmark data for the numerical results. Bearing this in mind, during the tests the barge was kept fixed and the geosim was attached to mechanical guiding arms, which restrained its sway, roll and yaw motions. Moreover, the geosim drift in surge was controlled by two springs linking the mechanical device to the model. This procedure enabled one to keep the gap width and length practically constant during the measurements, thus providing a convenient configuration for numerical modeling. Also for the purpose of calibration of the numerical methods, the mass of the guiding arms and the total mass and inertia of the complete system were determined and are presented in Table 2.

Table 1
Main characteristics of the barge and geosim.

Parameter	Barge	Geosim
Length overall [m]	1.67	2
Breadth [m]	0.665	0.40
Depth [m]	0.205	0.32
Draft [m]	0.12	0.18
Displacement weight [kg]	133.26	83.30
CoG above baseline [m] (Exp)	–	0.181
GMt [m]	–	0.0350
GMl [m]	–	1.87
CoG from the stern [m]	0.835	0.802
Pitch radius of gyration [m]	–	0.56
Heave period [s]	–	0.95
Pitch period [s]	–	1.20

Table 2
Main characteristics of the geosim including the mechanical guiding arms data.

Feature	GEOSIM
Guiding arms mass [kg]	5.5
Total mass [kg]	88.80
Pitch radius of gyration [m]	0.598
Heave period [s]	0.95
Pitch period [s]	1.26

The geosim model was positioned in the tank with its longitudinal axis coincident with the longitudinal axis of the tank and the barge was located aside of the geosim, as represented in the sketch shown in Fig. 4.

Geosim heave and pitch motions were tracked by means of a laser system installed in the towing tank carriage. Additionally, four wave probes (P1, P2, P3 and P4, see Fig. 4) were used for monitoring the wave elevation in different locations, three of them being positioned inside the gap. The relative distances between the wave probes are presented in Table 3. Figs. 5 and 6 present

Table 3
Relative distances between the wave probes.

L(P1–P2) [m]	0.48
L(P2–P3) [m]	0.475
L(P3–P4) [m]	0.485
L(P4–Stern Geosim) [m]	0.28

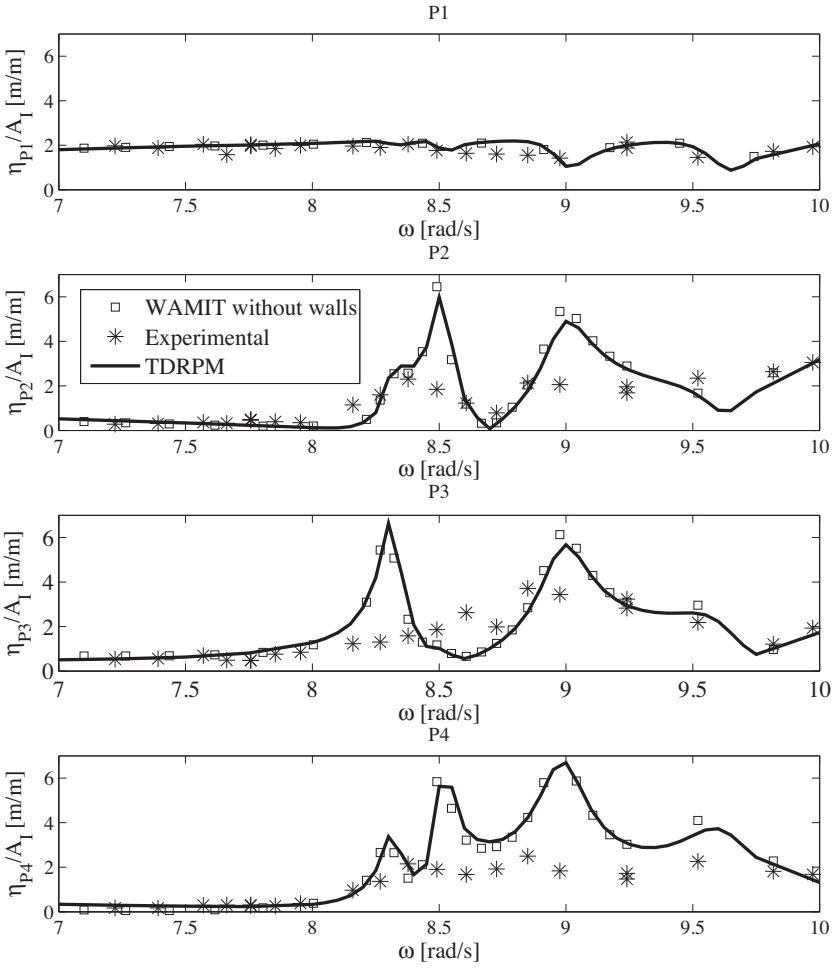

Fig. 15. Case 1: Comparison between WAMIT, TDRPM and experimental values in terms of wave elevations RAOs in different points positioned along the gap centerline. Gap width = 0.05 m.

two photographs of the experimental setup, including the probes arrangement.

Since the experiments were conducted in a towing tank, special care had to be taken in order to minimize the influence of reflected waves from the tank walls within the frequency range of interest (namely, the range where the gap resonant modes are expected to occur). In fact, the distance between the models was defined considering previous numerical results calculated by the software WAMIT, which aimed at evaluating the expected gap resonant frequencies and whether the presence of the tank walls would interfere with the experimental measurements at these frequencies. As will be demonstrated in the next section, by adopting proper gap widths, it was possible to restrict the influence of the tank walls to a range of frequencies different to the one in which we were interested in.

Once these preliminary investigations were performed, two experimental setups of gap widths 0.05 m and 0.10 m were selected and denoted as Cases 1 and 2, respectively. These tests were conducted focusing on the study of linear effects and included a set of 49 and 32 regular waves of small amplitude for Cases 1 and 2, respectively, where H is the wave height and λ is the wave length. The wave height for every frequency was determined considering a wave steepness smaller or equal to $H/\lambda \leq 3\,\%$ (limit established for the highest wave frequencies) and the maximum allowed wave height was 0.04 m in order to guarantee a stable propagation of the waves along the tank. For Case 1, which was tested first, the number of waves was larger because some of them were used with the intent of evaluating the influence of the tank walls and also checking whether the preliminary numerical models were providing reasonable results. For Case 2 the test matrix was reduced to 32 waves, concentrating most of the waves within the frequency range where gap resonance had been predicted by the numerical models. Due to the limitations concerning the width of the towing tank, only head waves were considered.

Finally, before moving to the discussion of the numerical models employed in this study, a comment on the model scale is necessary. The size of the models and their geometries were chosen based exclusively on the tank dimensions and on the equipment available for the tests. Although it is for sure tempting to try to extrapolate these dimensions to a full-scale side-by-side operation, one must have in mind that the prime objective of the study was to create appropriate conditions for an adequate verification of the numerical method in the towing tank scale. This is even more important when one reminds that the damping emulation methods adopted to "correct" the potential flow results do not allow for a straightforward extrapolation of the results obtained in the tank. Considering all that has been said, however, one may also notice that at least some relevant full-scale information can be obtained from the tests. As an exercise, if one considers a 1:150 scale factor, then the length of the geosim in full-scale would be 300 m, which may be considered a reasonable value for LNG ship vessels. In addition, as will be further presented in this paper, the computational results indicated that, for the multi-body configurations here studied, the gap resonant frequencies are expected to occur around 8.0 s (in full-scale),

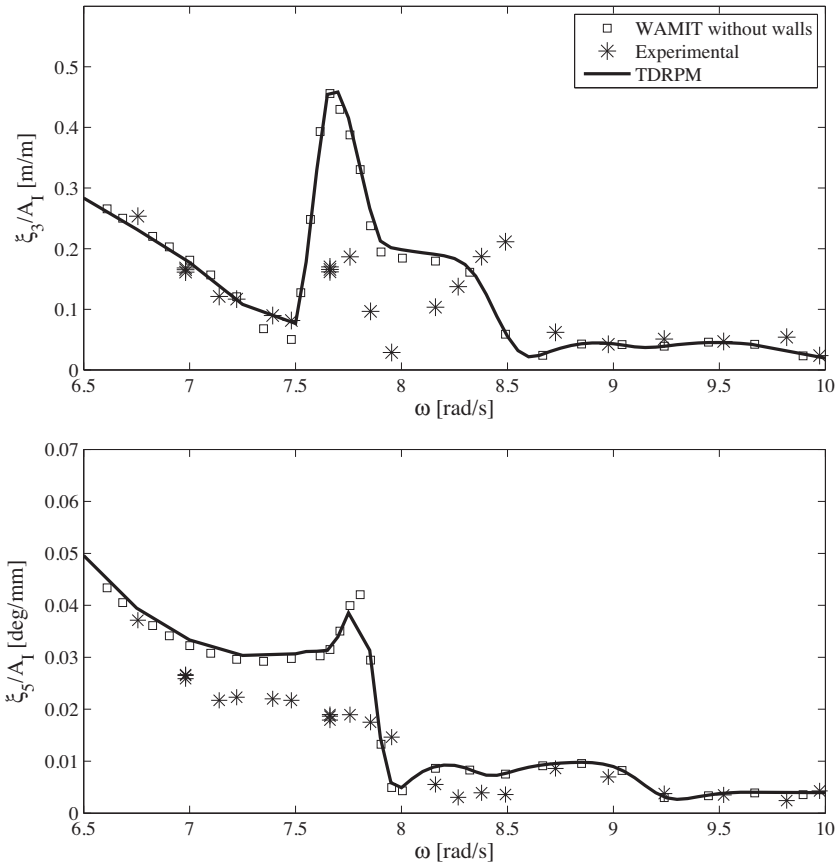

Fig. 16. Case 2: Comparison between WAMIT, TDRPM and experimental values in terms of heave (top) and pitch (bottom) RAOs. Gap width = 0.1 m.

which may be considered as a typical operational peak period for sea waves.

3. Numerical models

3.1. WAMIT numerical models

The higher order WAMIT module was applied with the intent of providing preliminary information regarding the characterization of the gap resonant frequency ranges, thus enabling the definition of the gap widths and regular waves to be tested experimentally as well as the investigation of the influence of the tank walls on the results. Since WAMIT is formulated in frequency domain and applies the well known free surface Green function, which eliminates the necessity of discretizing the free surface, the code is more suitable to be used for exhaustive variations of important parameters that must be assessed in the problem, if compared to the TDRPM solver.

For this analysis, numerical models with and without tank walls were computed in WAMIT. The numerical models with the tank walls were emulated for both cases (1 and 2) by introducing sets of bodies images (barge + geosim) with respect to the vertical symmetry planes. Moreover, since two tank walls should be considered and the exact solution of the problem would only be reached by using an infinite series of images, a convergence analysis was performed in order to determine the minimum number of images above which the results would not be significantly affected. In total, 5 sets of body images had to be considered for achieving a reasonable convergence, resulting in a model composed of 12 bodies, which was than solved by considering 6 bodies plus the symmetry plane. In order to illustrate the models, the symmetries are represented in Fig. 7.

Concerning the bodies meshes, the *panel size* parameter was set to 0.1 and 0.2 for the cases 1 and 2, respectively, values that were defined after a convergence analysis of the mesh. One should notice that a smaller value of panel size was required for case 1, since the gap width was smaller.

3.1.1. Investigation of the tank walls effects

Fig. 8 presents a comparison between RAO calculations with the WAMIT model and the measured data for Case 1. The comparison refers to the geosim heave and pitch RAOs and shows that the heave motion amplifications observed in the experiment for frequencies between 3.5 and 7.0 rad/s are caused by waves reflected by the tank walls. The evidence for this comes from the fact that the WAMIT numerical model with walls was indeed able to capture the same trends of the experimental curve. Moreover, one should also notice that the influence of the walls tends to be minimized for higher frequencies (>7 rad/s), for which both WAMIT numerical models present similar results. It is also worth mentioning that the pitch motion is not significantly affected by the presence of the walls.

The influence of the tank walls on the wave elevations at the gap centerline is investigated in Fig. 9, from which it can be inferred that the wall effects are of minor degree. Both WAMIT numerical models (with and without walls) present good agreement with the experimental data for wave frequencies lower than <8 rad/s, in the same range where the heave motions are significantly influenced by the tank walls. Nonetheless, one should realize that the numerical results provided by both models (with and without walls) present significant wave amplifications for a range of frequencies

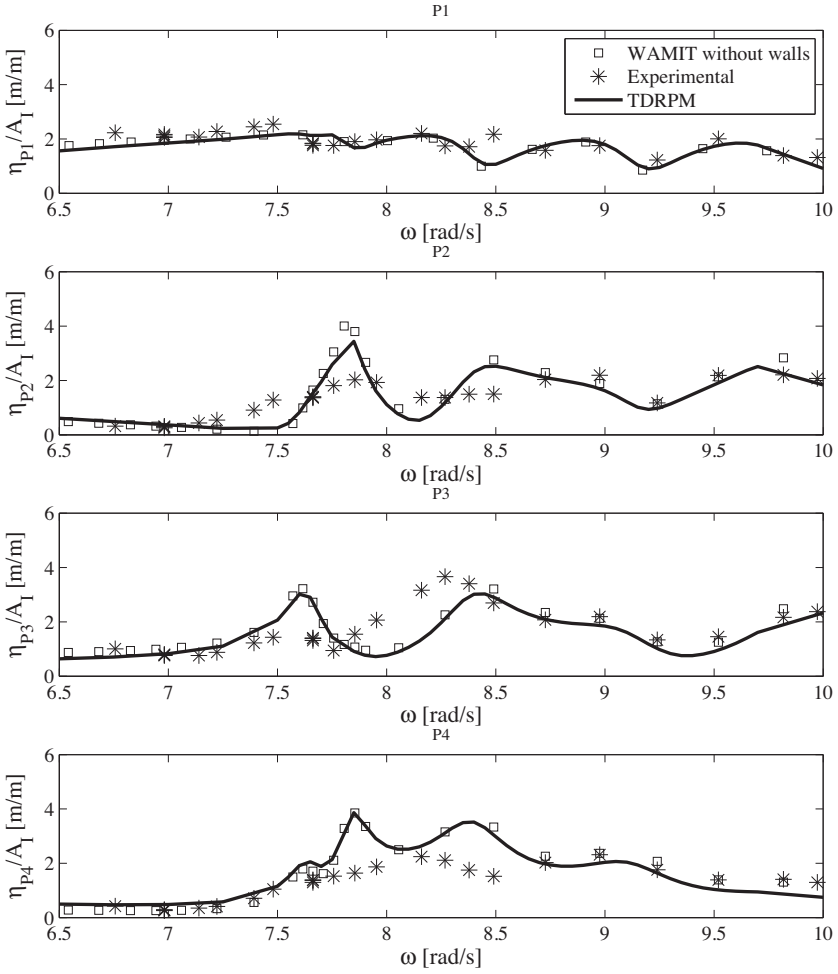

Fig. 17. Case 2: Comparison between WAMIT, TDRPM and experimental values in terms of wave elevations RAOs in different points positioned along the gap centerline. Gap width = 0.1 m.

between 8.0 and 9.0 rad/s, which are in general much larger than the observed experimental values.

As aforementioned, potential flow solvers present some difficulties when dealing with physical problems that contain narrow gaps, tending to provide unrealistic wave elevations and body motions for the associated gap resonant frequencies, where the potential flow physics is not enough to represent the hydrodynamic phenomenon. A more complete discussion about this issue will be presented in the next sections, along with the description of the numerical modeling based on the time domain solver.

Analogous results for Case 2 are presented in Figs. 10 and 11. By analyzing both figures, it is possible to observe that the results present a behavior similar to the ones obtained for Case 1, once again emphasizing that the influence of the tank walls is more pronounced for wave frequencies lower than 7.0 rad/s.

Based on these analyses, it was possible to conclude that although the experimental data was conducted in a towing tank with walls relatively close to the model bodies, the influence of reflected waves was restricted to frequencies below the range of main interest to this study, namely the range where gap resonant effects are caused by the hydrodynamic interaction of the models in side-by-side configuration.

3.2. Time domain Rankine panel method (TDRPM)

A novel linear TDRPM developed by the Numerical Offshore Tank of the University of Sao Paulo [28] is also applied for calculating the first order geosim motions and wave elevations in the gap. Details of the method are presented in Appendix A, so only the main features of the method will be described next, for the sake of conciseness. The code is based on the three-dimensional low order panel method and applies the Rankine source as Green's function. In this version, the nonlinear effects originated from the presence of unknown free surface and body surface positions are neglected. The robust and accurate solution of this linear problem is a very useful first stage before dealing with more complex nonlinear problems. However, the nonlinear extension of the code is already under development, in which the lower order approach will be substituted by a higher order description of both the body geometry and variable quantities in order to improve the accuracy of the spatial derivatives inherent to the mathematical problem.

In a time domain simulation it is essential to solve the equations of the flow and of the body motions simultaneously, since one needs to guarantee a dynamic equilibrium of forces between the fluid and the floating body at all times. In this approach, the simulations require an accurate prediction of the pressure field for all time-steps in order to guarantee a consistent and stable numerical solution, especially when free floating bodies are being assessed. Poor estimations of the pressure variation by finite difference schemes normally give rise to numerical instabilities [32].

In order to deal with this problem, the present TDRPM solves two complementary boundary value problems defined for the velocity and acceleration potentials, the latter being used to avoid the

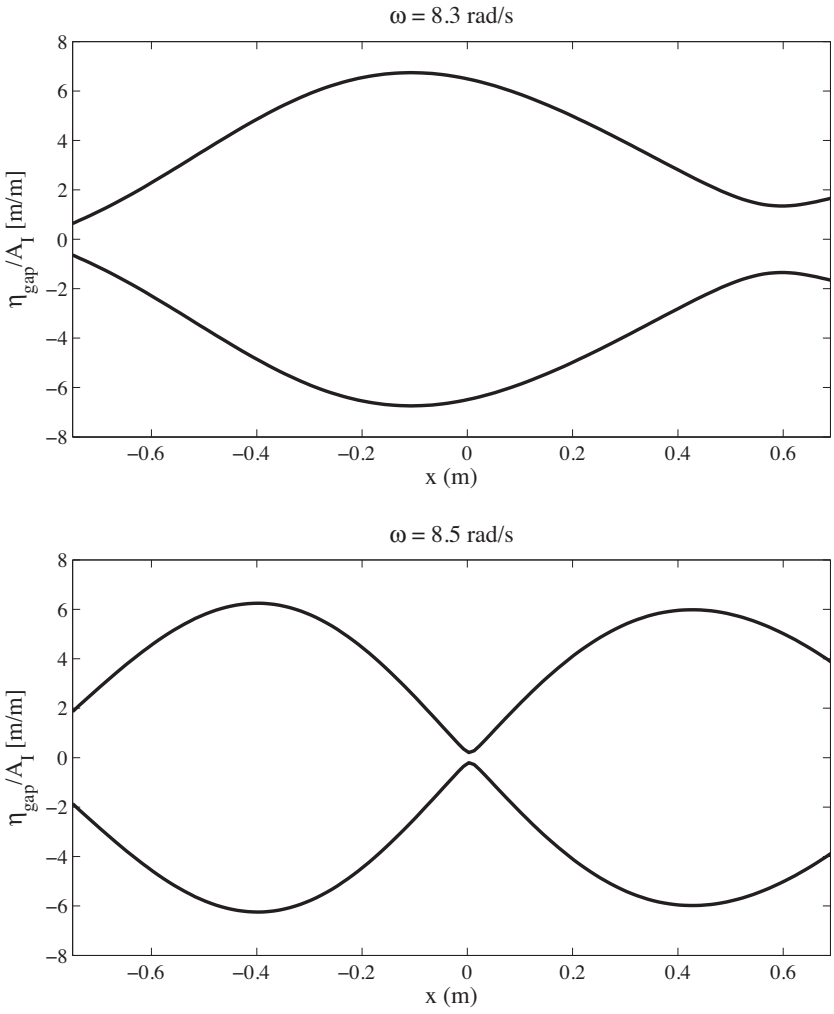

Fig. 18. Case 1: Gap wave elevation envelopes in spatial domain computed with TDRPM. Incoming wave frequencies $\omega = 8.3$ rad/s (top) and $\omega = 8.5$ rad/s (bottom). Wave propagates from positive to negative x coordinates. Gap width = 0.05 m.

aforementioned numerical problems in calculating the time derivatives of the velocity potential. More specifically, the method applies the implicit boundary condition method presented by van Daalen [32] and Tanizawa [33].

The time-marching of the problem is performed by a fourth order Runge Kutta method (RK4), which provides high accuracy and stability to the algorithm. The simulations are initialized with a ramp function in order to avoid impulsive responses in the domain, since they could induce long transient periods with no physical interest to our analysis. Furthermore, a numerical damping zone is applied to account for wave dissipation in the far field part of the free surface, so that waves reflected from the domain boundaries will not disturb the solution.

3.2.1. Damping lid approach

Numerical methods based on the potential flow theory are known to have a poor performance when dealing with multiple bodies arranged in a side-by-side configuration, tending to provide unrealistically high wave elevations in the gap between the vessels, which lead to poor estimations of forces and motions. In practice, the wave elevations would be limited by viscous effects that are not accounted for by potential flow solvers. In this regard, the application of suppression methods to handle these gap resonant problem becomes an interesting alternative for a better representation of the physical problem.

In addition to the unrealistic values observed when the mathematical problem is solved in time domain, a very slow numerical convergence for frequencies near the resonant ones is also observed. In these cases, a considerable number of wave cycles is necessary to reach a steady state.

In order to deal with these gap resonant effects, we present a new development in the TDRPM, in which the free surface boundary conditions (kinematic and dynamic) are reformulated by means of the damping lid technique used in frequency domain by Chen [15], Fournier et al. [16], Pauw et al. [17] and Bunnik et al. [18]. In this method, a constant damping factor ϵ is included in the free surface boundary conditions ((A.4) and (A.5)), as presented in Eqs. (1) and (2):

$$\frac{\partial \eta}{\partial t} = \frac{\partial \phi}{\partial z} - \epsilon \eta \quad \text{on} \quad z = 0 \quad \text{in} \quad \text{the} \quad \text{gap}, \tag{1}$$

$$\frac{\partial \phi}{\partial t} = -\eta g - \epsilon \phi \quad \text{on} \quad z = 0 \quad \text{in} \quad \text{the} \quad \text{gap}. \tag{2}$$

One should notice that the undamped free surface elevation is recovered by setting the damping factor ϵ equal to zero. As will be heuristically demonstrated later in the paper, the imposition of the damping parameter attenuates the numerical convergence problems, stabilizing the solutions much faster. Another characteristic of the method is that the damping parameter influences the results only in the resonant frequency range. Moreover, one of the main

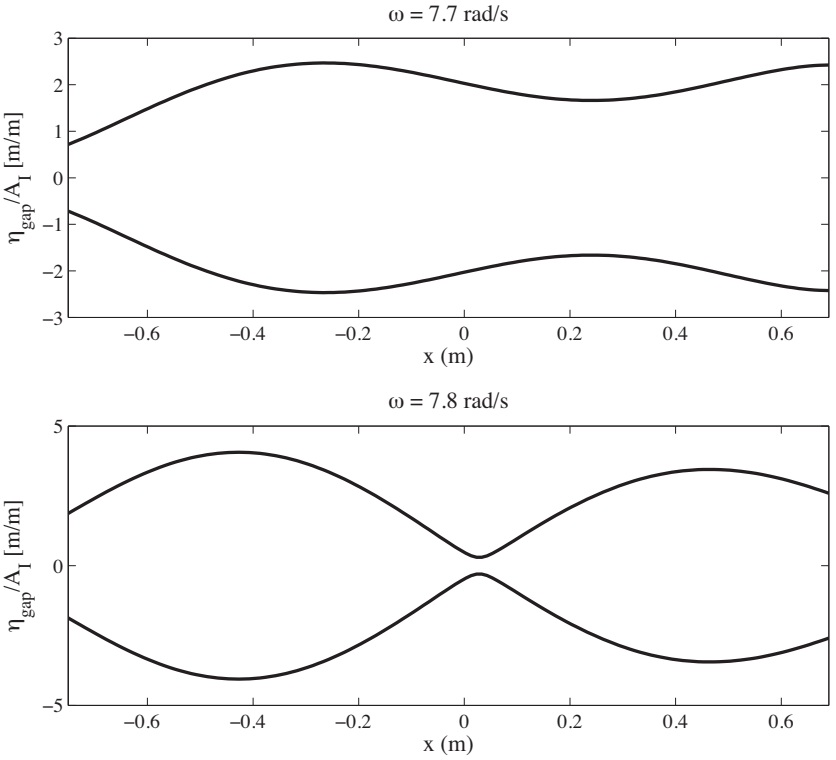

Fig. 19. Case 2: Gap wave elevation envelopes in spatial domain computed with TDRPM. Incoming wave frequencies $\omega = 7.7$ rad/s (top) and $\omega = 7.8$ rad/s (bottom). Wave propagates from positive to negative x coordinates. Gap width = 0.10 m.

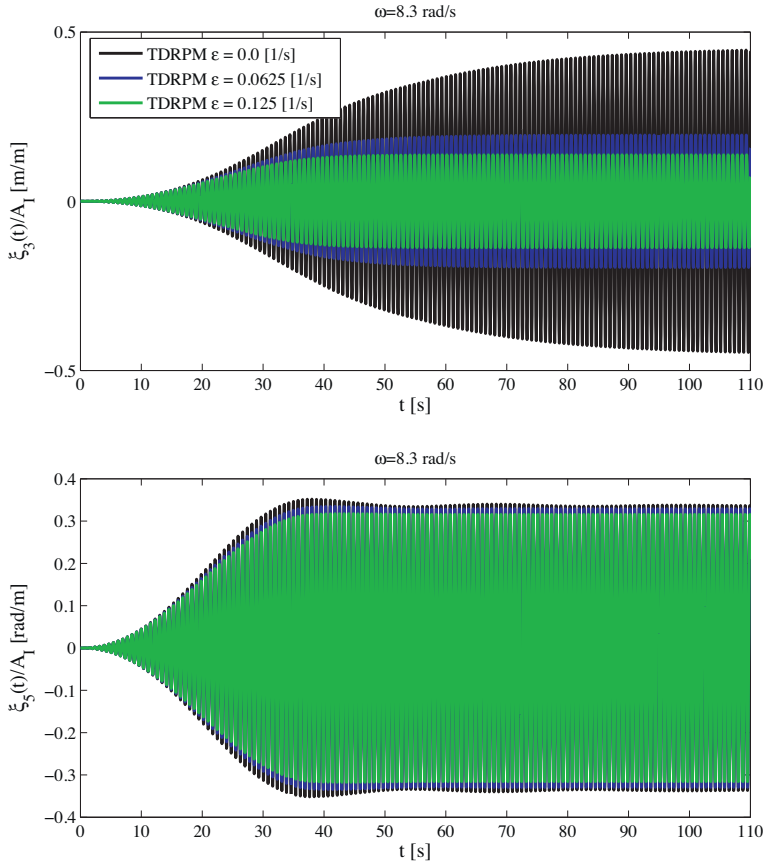

Fig. 20. Case 1: Heave (top) and pitch (bottom) motions time series, computed with TDRPM, for different values of damping factor ϵ. Incoming wave frequency $\omega = 8.3$ rad/s. Gap width = 0.05 m.

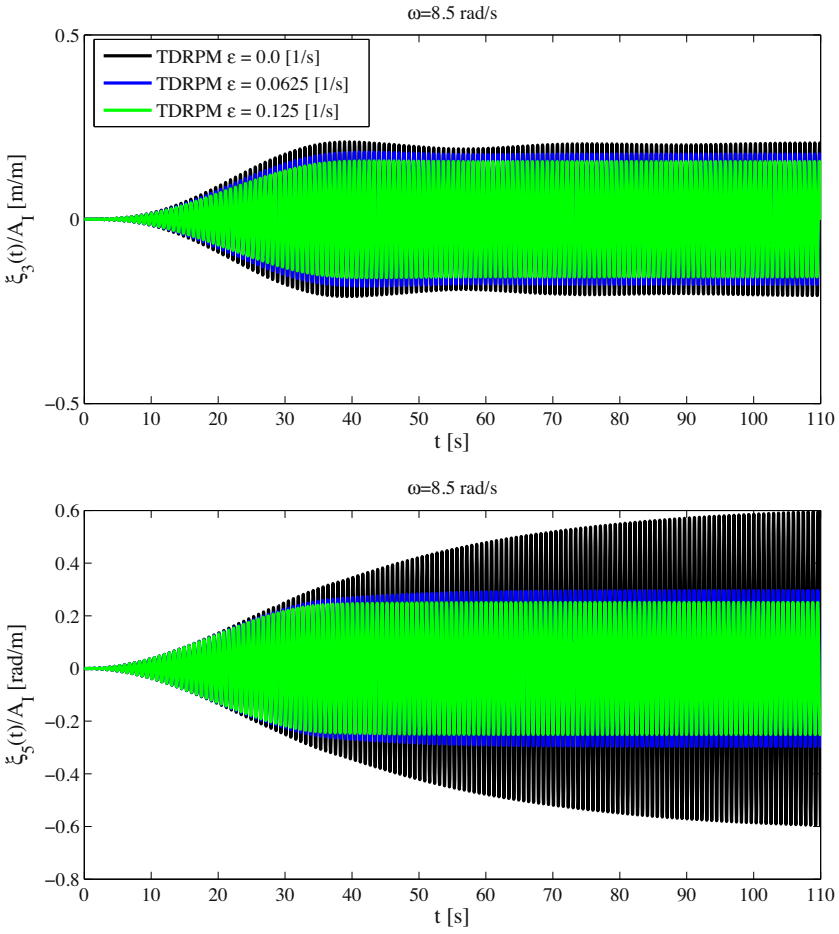

Fig. 21. Case 1: Heave (top) and pitch (bottom) motions time series, computed with TDRPM, for different values of damping factor ϵ. Incoming wave frequency $\omega = 8.5$ rad/s. Gap width = 0.05 m.

advantages of this method is that it does not require the use of additional degrees of freedom in the model, as the technique applied by Newman [14]. Instead, only one value of damping factor is included in the free surface boundary conditions.

On the other hand, it is important to mention that the ϵ value is, for the moment, not defined rationally, but it is merely "tuned" with the experimental data considering that the coefficient depends neither on the wave amplitude or frequency. Despite the simplicity of this technique, it will be shown that reasonable results can be obtained in terms of wave elevations and body motions in most of the cases.

4. Results

4.1. TDRPM grids for the case studies

The barge and geosim hulls were modeled with 1584 and 1504 quadrangular panels, respectively. For the free surface meshes, 4797 panels were applied in Case 1 and 5751 panels in Case 2, the difference being associated exclusively to the number of panels required to model the gap surface (750 panels for Case 1 and 1500 for Case 2). These values were obtained after a convergence analysis in terms of the geosim motions and wave elevations.

Since the analysis conducted with WAMIT did not indicate significant wall effects in the gap resonant frequencies, the walls have been neglected in the TDRPM simulations, thus reducing significantly the number of panels and, consequently, the total processing time.

By taking Case 1 (gap equal to 0.05 m) as an example, Figs. 12 and 13 present the bodies (with the gap) and free surface meshes used in the TDRPM computations, respectively. Notice that the meshes have been refined towards the bodies edges, with a larger concentration of panels near the gap region in order to improve the numerical convergence. In addition, the free surface mesh has been designed to allow a smooth transition from the gap region to the outer free surface. The same mesh topology has been applied in Case 2.

The TDRPM has been run for several regular wave frequencies within the range of frequencies tested experimentally. Each simulation has provided a set of time series describing the geosim motions in the 3 D.O.F. (surge, heave and pitch) and the wave elevation at the wave probes locations (Table 3), from which the signal amplitudes have been characterized with the root mean square (rms) from a steady state interval. The time-step of each simulation has been set to $\Delta t = T/30$ s, whereas the numerical damping zone has been set with a length equal to $b = 2\lambda$ and intensity $a = 1.5$ for all cases (see A). Moreover, three different values of damping factors $\epsilon = (0, 0.0625, 0.125)$ [1/s] applied in the gap between the bodies have been investigated. In this relations, T and λ refer to the incident wave period and length, respectively.

4.2. Comparisons between TDRPM, WAMIT and experimental data

The comparison between TDRPM, WAMIT and experimental results in terms of geosim motions and wave elevations for Case

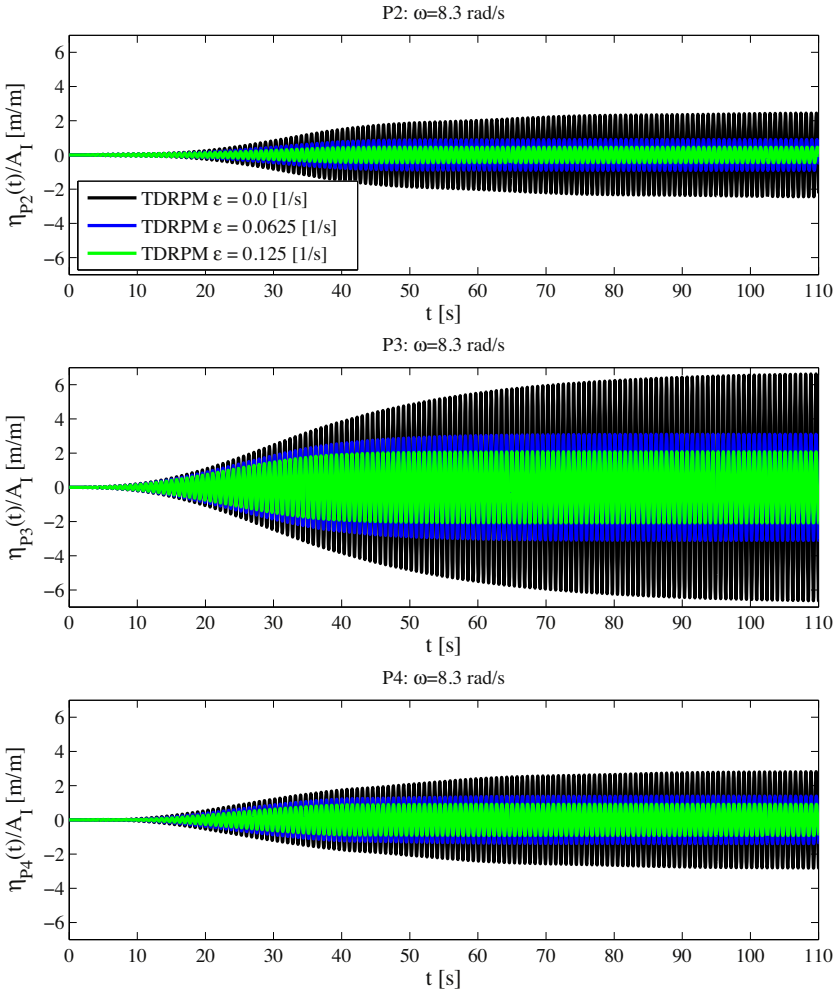

Fig. 22. Case 1: Wave elevation time series, computed with TDRPM, at P2 (top), P3 (middle) and P4 (bottom) for different values of damping factors ϵ. Incoming wave frequency $\omega = 8.3$ rad/s. Gap width = 0.05 m.

1 are presented in Figs. 14 and 15, whereas for Case 2 they are presented in Figs. 16 and 17. One should notice that only the WAMIT model without walls is being considered, since the results are focused exclusively on the range of frequencies in which the influence of tank walls can be disregarded (see Section 3.1.1).

The overall agreement between TDRPM and WAMIT results is good for all the RAO curves. Even considering the fact that the TDRPM is formulated in time domain, such an agreement was indeed expected since the boundary value problem solved by both computational codes is exactly the same when the damping factor ϵ is equal to zero. Also, it is clear that the numerical results tend to overestimate, in both cases, the experimental data for some frequency intervals.

For Case 1 (Fig. 14), one should notice that in the frequency range 8–9 rad/s there is a numerical resonance, which may be identified by the spurious peaks in the heave and pitch RAOs at approximately 8.3 and 8.5 rad/s, respectively. The same trends are observed for the wave elevations RAOs (Fig. 15), especially for the measurement points that are in fact inside the gap between the bodies (P2, P3 and P4). Since the wave probe P1 was positioned outside the gap, it does not present significant influence from the resonant effects, resulting in a smoother RAO curve when compared to the other probes. At this location, a perfect agreement between numerical and experimental results was observed.

The wave modes associated to the resonant frequencies of 8.3 and 8.5 rad/s are presented in Fig. 18, which illustrates the envelopes of wave elevation inside the gap in spatial domain calculated by the TDRPM for Case 1. For the resonant wave frequency 8.3 rad/s, it is possible to observe that the wave elevation in the gap presents a piston type resonant mode, in which the wave behaves like a column of water moving up and down in the region between the vessels [4]. Regarding the resonant frequency 8.5 rad/s, one may realize that instead of a piston mode, a second longitudinal mode is visualized. It is interesting to observe that this mode is related to the spurious amplification of the pitch motion at this same frequency (Fig. 14).

The same qualitative behavior observed for Case 1 may be stated for Case 2 (Figs. 16 and 17). In this case, however, since the gap width was increased to 0.10 m, the numerical resonant frequencies are slightly shifted towards lower frequencies 7.5–8.5 rad/s. In this configuration, the numerical resonant peaks for heave and pitch RAOs are approximately 7.7 and 7.8 rad/s. Once again, these resonant frequencies coincide with the piston and second longitudinal modes of the gap, respectively, as may be observed in Fig. 19. It is also interesting to observe that, for waves that are outside of the gap resonant frequency range, the numerical results agree with the experimental data very well.

4.3. TDRPM model with damping lid

As an attempt to improve the numerical results for the geosim motions and wave elevations within the resonant ranges, the

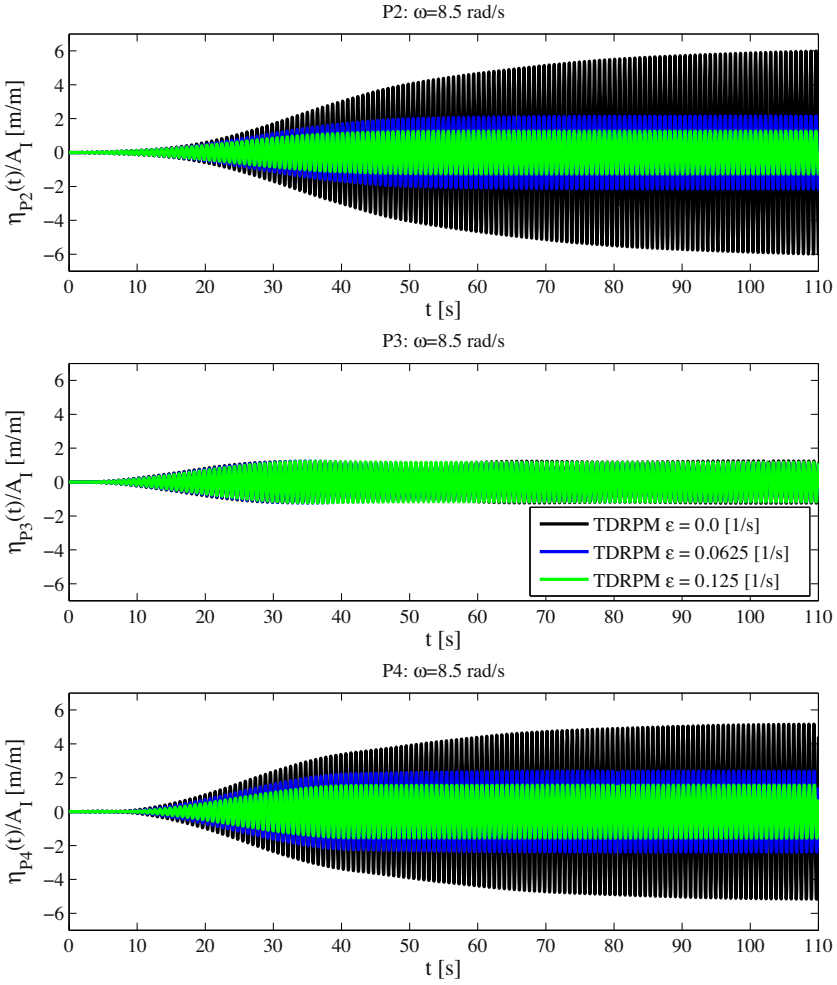

Fig. 23. Case 1: Wave elevation time series, computed with TDRPM, at P2 (top), P3 (middle) and P4 (bottom) for different values of damping factors ϵ. Incoming wave frequency $\omega = 8.5$ rad/s. Gap width = 0.05 m.

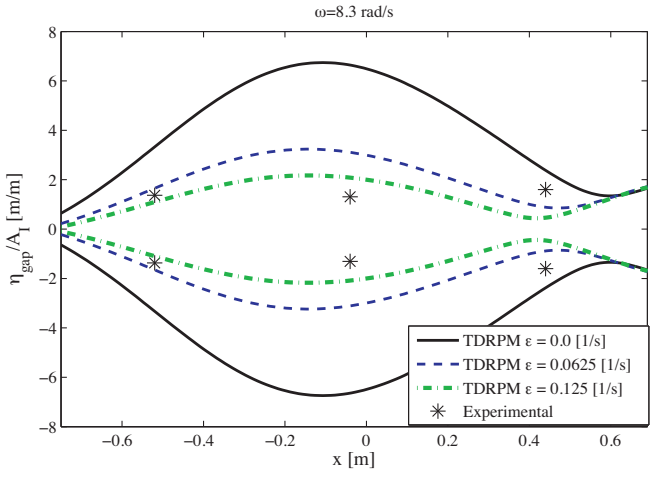

Fig. 24. Case 1: TDRPM and experimental comparisons of the gap wave elevation envelopes in spatial domain for different values of damping factors ϵ. Incoming wave frequency $\omega = 8.3$ rad/s. Wave propagates from positive to negative x coordinates. Gap width = 0.05 m.

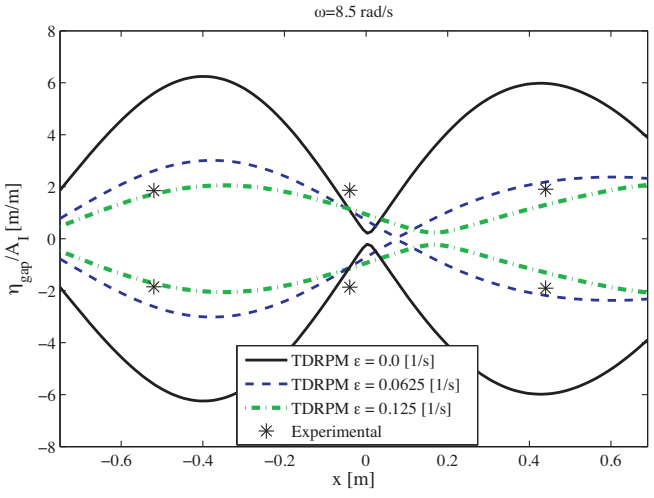

Fig. 25. Case 1: TDRPM and experimental comparisons of the gap wave elevation envelopes in spatial domain for different values of damping factors ϵ. Incoming wave frequency $\omega = 8.5$ rad/s. Wave propagates from positive to negative x coordinates. Gap width = 0.05 m.

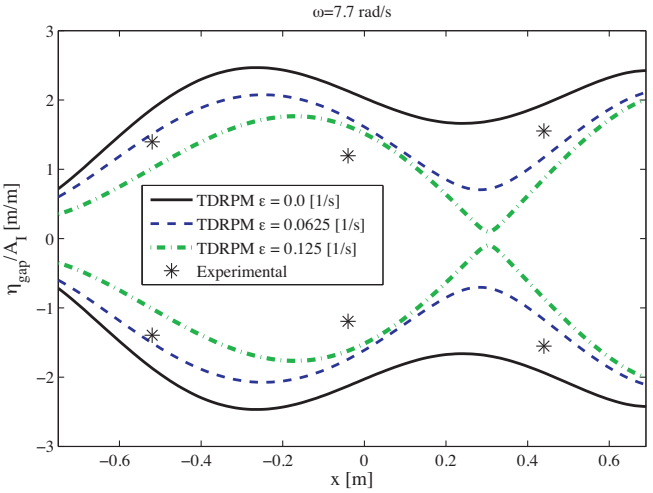

Fig. 26. Case 2: TDRPM and experimental comparisons of the gap wave elevation envelopes in spatial domain for different values of damping factors ϵ. Incoming wave frequency $\omega = 7.7$ rad/s. Wave propagates from positive to negative x coordinates. Gap width = 0.10 m.

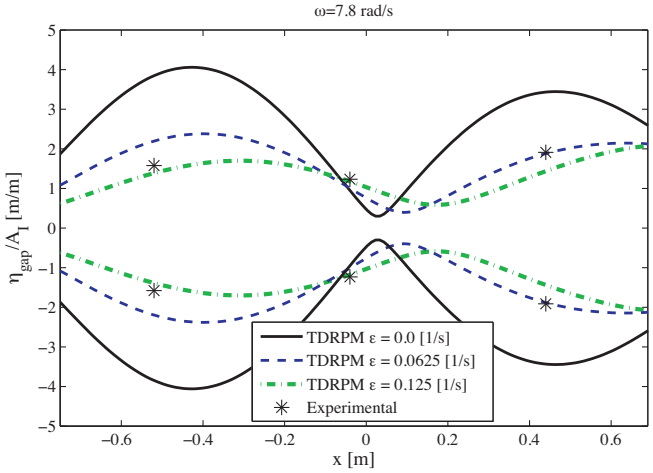

Fig. 27. Case 2: TDRPM and experimental comparisons of the gap wave elevation envelopes in spatial domain for different values of damping factors ϵ. Incoming wave frequency $\omega = 7.8$ rad/s. Wave propagates from positive to negative x coordinates. Gap width = 0.10 m.

results obtained with the TDRPM code with the damping lid model discussed in Section 3.2.1 are presented in this section. For comparison purposes only three different damping factors have been used $\epsilon = (0.0, 0.0625, 0.125)$ 1/s.

First, a sensitivity analysis concerning the behavior of the time series of motions and wave elevations with respect to the varying damping factor ϵ is presented. Considering as an example the results of Case 1, Figs. 20 and 21 display the histories for heave and pitch motions considering waves with frequencies 8.3 and 8.5 rad/s, which correspond to the gap resonant frequencies for heave and pitch motions, respectively. The results show that the imposition of a damping factor on the gap is effective in reducing the amplitudes of heave and pitch motions at their respective resonant frequencies. Notice that, for the wave frequency of 8.3 rad/s (heave resonance frequency), the amplitudes of the pitch motions are not affected by the variation of ϵ values, while the opposite occurs for the heave motion when the wave frequency of 8.5 rad/s (pitch resonance frequency) is considered.

The time series of wave elevations at points P2, P3 and P4 are presented in Figs. 22 and 23 for the wave frequencies 8.3 and 8.5 rad/s, respectively. As for the geosim motions, the use of the damping lid technique reduces the wave amplitudes in the gap, which is a good indication that the method may be used in order to more closely emulate the wave behavior observed in the experiments more closely.

One should also realize that the inclusion of the damping factor in the formulation clearly favors the convergence of the time series (Figs. 22 and 23). It is possible to observe that the time series obtained with non-zero ϵ values reached a steady state much faster than the cases with zero ϵ. In fact, with zero ϵ more than 150 wave cycles in the simulation were necessary to stabilize the motions and wave elevations. This behavior is analogous for the motions and wave elevations obtained in Case 2.

The associated envelopes of wave elevation in the gap for Case 1 are presented in Figs. 24 and 25. In these figures, the experimental amplitudes of the three monitored points in the gap are also included for comparison purposes. It can be noticed that the

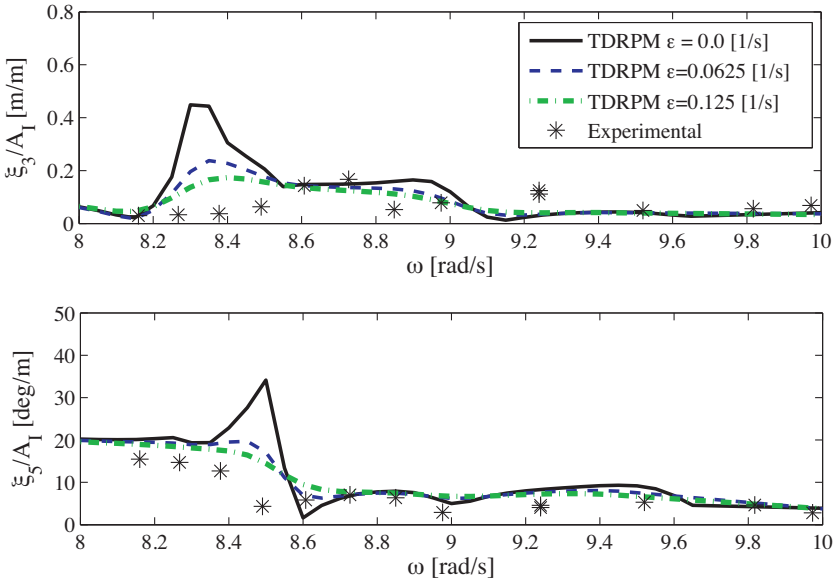

Fig. 28. Case 1: TDRPM and experimental comparisons in terms of heave (top) and pitch (bottom) motions RAOs for different values of damping factors ϵ. Gap width = 0.05 m.

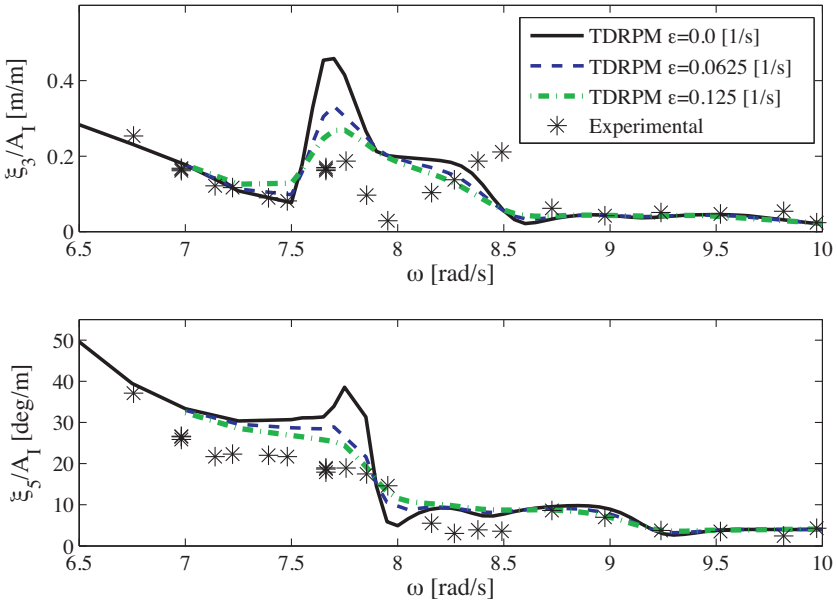

Fig. 29. Case 2: TDRPM and experimental comparisons in terms of heave (top) and pitch (bottom) motions RAOs for different values of damping factors ϵ. Gap width = 0.10 m.

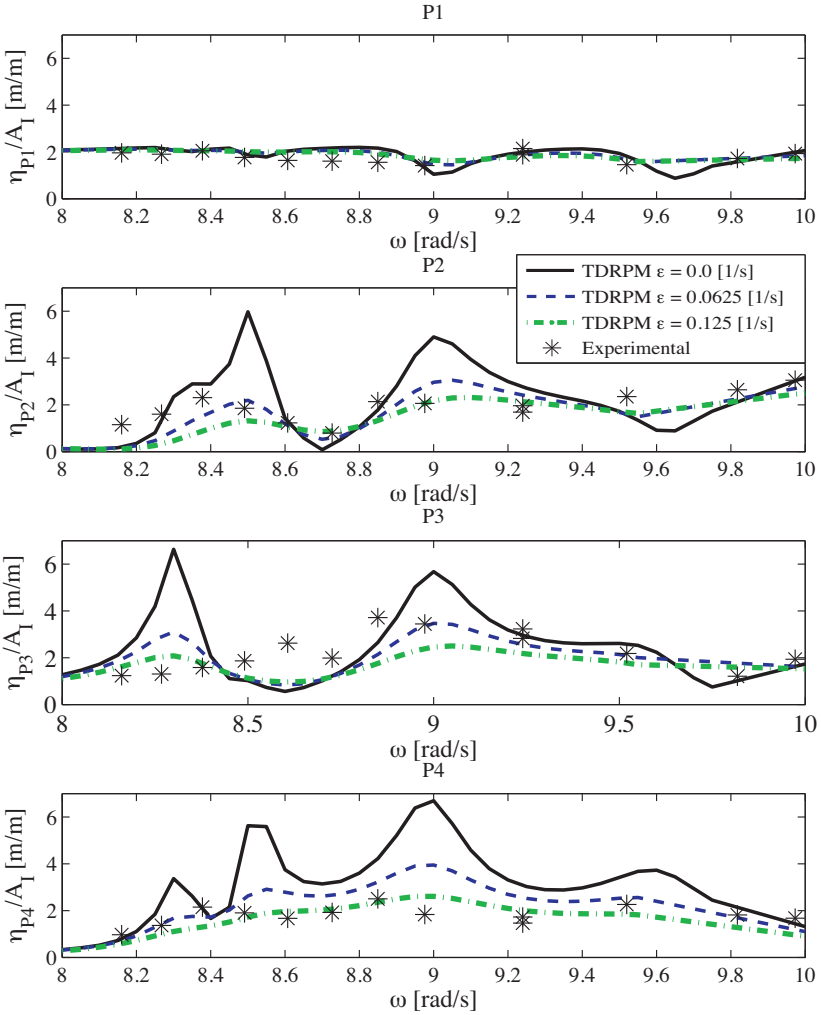

Fig. 30. Case 1: TDRPM and experimental comparisons of wave elevations in the gap for different values of damping factors ϵ. Gap width = 0.05 m.

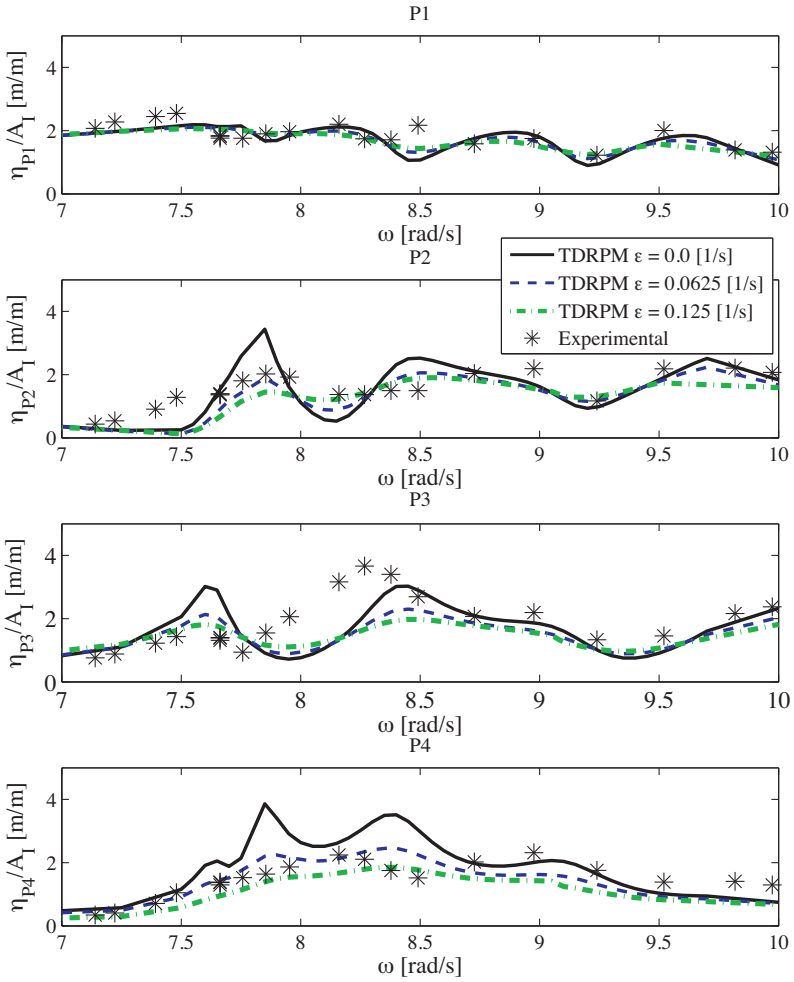

Fig. 31. Case 2: TDRPM and experimental comparisons of wave elevations in the gap for different values of damping factors ϵ. Gap width = 0.10 m.

damping lid technique implemented in this work greatly improved the results, presenting a much better agreement between the computed wave elevations and the experimental data, especially for the damping factor value of $\epsilon = 0.125$ 1/s, which provided the best fit with the measured data.

Figs. 26 and 27 present the wave elevation envelopes for Case 2, considering the resonant frequencies $\omega = 7.7$ and $\omega = 7.8$ rad/s. Once more, the damping technique provides a considerable improvement to the wave profile patterns in the gap, reproducing the test data reasonably well. In this case, the damping factor $\epsilon = 0.0625$ 1/s presented a slightly better performance in relation to $\epsilon = 0.125$ 1/s.

The influence of the damping factors on the motions RAOs is presented in Figs. 28 and 29 for Cases 1 and 2, respectively. In general, the damping factor decreases the resonant values in the frequency range of interest, eliminating the spurious characteristic of the curves. Nevertheless, in both cases, the numerical results of heave motion present different trends when compared to the experimental data. Regarding the pitch motions, the inclusion of the damping coefficient improves the matching with the test data, recovering the trends of the RAOs.

For the wave elevations RAOs in the gap, presented in Figs. 30 and 31, the use of the damping factor also improved the predicted wave amplitudes in comparison to the measured data, eliminating most of the irregular oscillations observed for $\epsilon = 0.0$ 1/s. For probes P2 and P4, the application of the method enabled to recover the wave amplitudes inside the gap reasonably well. Concerning P3, a larger discrepancy between the results is observed, since the experimental data presented higher elevations in comparison with TDRPM even without the inclusion of a damping factor. It is also noticeable that all the TDRPM results tend to the same asymptotic value when the waves are outside of the resonant frequency range. In addition, it is possible to observe that the inclusion of different damping values did not modify the resonant frequencies.

One should notice, however, that although the damping lid method applied does not intend to capture the physics of the flow in the gap, the use of this simplified technique, which incorporates damping factors independent on the wave amplitudes and frequencies, has provided reasonable numerical results with a fair agreement with the experimental data for most of the cases. Overall, in terms of the motions and wave elevations, the value of damping of $\epsilon = 0.125$ 1/s has provided the best agreement with the test results in general.

5. Conclusions

The hydrodynamic interaction of two ships arranged in side-by-side configuration considering two gap widths has been analyzed using an in-house developed time domain Rankine panel method.

The numerical results have been compared to seakeeping tests conceived in a very fundamental setup, assuming a fixed barge

and restraining the geosim motions to surge, heave and pitch only. Through this approach, the gap width was kept fixed during the measurements, providing an adequate scenario for the numerical method. Tests have been carried out with two gap distances defined in a preliminary numerical analysis conducted with the frequency domain software WAMIT. Since the tests have been performed in a towing tank, special care has been taken in order to avoid the influence of the tank walls on the results, especially in the range of frequencies where gap resonant modes are expected to occur.

Results have been discussed in terms of the geosim motions and wave amplitudes in the gap. Both TDRPM and WAMIT presented undesirable overestimations of the experimental values for a range of frequencies, which are dependent on the gap width. In fact, the numerical and experimental results have shown that the resonant frequencies were lower for the system with the largest gap width.

Different resonant frequencies have been observed for heave and pitch motions. As demonstrated by the wave envelopes inside the gap computed by the TDRPM, the heave motion is significantly amplified due to the presence of a piston-type mode inside the gap, whereas the pitch motion is influenced by the occurrence of a second longitudinal mode. The same conclusions could be drawn in this respect for both gap widths.

The TDRPM solver presented numerical convergence problems when simulating wave frequencies near to the resonant ones. In these cases, the motions and wave elevations time series showed a long transient period, attesting the numerical problems to reach the steady-state. This problem has been solved by the application of a damping lid method, which incorporates a damping factor in the free surface boundary conditions. By considering this method, the time series reaches the steady state much faster. This is indeed a positive indication regarding future applications of the method to the analysis of multi-vessels in irregular wave conditions. In addition, despite the simplicity of the damping model, the use of the damping lid technique has also improved the numerical results, reducing the discrepancies observed with the experimental data. Nevertheless, it should be noticed that the choice of the damping parameter has been done heuristically and for a better insight about the influence of this parameter on the numerical solutions, further analysis is still required.

Concerning future improvements of the TDRPM numerical model, a new version of the code with the inclusion of a second order module for the calculation of drift forces is under development. Algorithms for representing both the body geometry and the velocity potential, in a higher-order numerical scheme using NURBS functions is ready and the nonlinear model is currently being implemented. This new version will enable the future evaluation of the damping lid method not only in terms of first order quantities, but also its effects on the second-order forces, which are also supposed to play an important role in practical side-by-side offloading operations.

Another topic of interest concerns the investigation of the problem not only under the view of the potential flow theory, but also applying viscous CFD numerical tools in order to have a better insight of the physical behavior of the problem, especially, regarding the influence of different bilge geometries, which are known to be important parameters for the flow in the gap [10,11]. In fact, this approach might also be envisaged with the purpose of calibration of the present damping lid method, which, nowadays, must be adjusted based on results obtained in particular scaled model tests. Indeed, Molin et al. [10] showed that a better agreement between potential flow results and experimental data is obtained when the models present a rounded shape bilge, which is a good indication that the damping values is affected by the model geometries. In addition, the application of CFD tools could also be used with the intent of defining an appropriate methodology to extrapolate the damping values tuned with model test data to full scale dimensions, which is a complex issue not yet well defined. Nevertheless, one must keep in mind that the application of CFD simulations for this kind of problem is very time consuming and requires the implementation of sophisticated algorithms to deal with multi-body problems in free floating condition. Moreover, this difficulty is even more evident when using viscous flow solvers for full scale simulations, since in order to keep enough grid resolution the number of cells increases as approximately the square of Reynolds number.

Acknowledgments

The authors gratefully acknowledge to CEHINAV Research Group and Numerical Offshore Tank (TPN) for funding and professional support. Rafael A. Watai and Felipe Ruggeri acknowledge FAPESP for the scholarship grants (2010/08778-2) and (2012/06681-7), respectively. The authors are thankful to Prof. Luis Pérez Rojas, Prof. Jesus Gómez-Goñi, Hugo Ramos-Castro, Benjamin Bouscasse, Gabriele Bulian, Pedro Cardoso de Mello, Juan Luis Chácon-López and Ricardo Abad for the model setup contribution.

Appendix A. Time domain Rankine panel method

A.1. Theoretical formulation

The mathematical description of the physical problem here addressed considers the same situation tested in the towing tank (Section 2), which comprises two bodies with zero forward speed, being one fixed and the other free to oscillate in surge, heave and pitch. Moreover, the system is arranged in a side-by-side configuration and is subjected to the action of incoming gravity waves that may be assumed to be propagating in infinity fluid.

The flow is assumed irrotational and incompressible whereas the fluid is assumed inviscid and homogeneous, allowing the problem to be solved under the hypothesis of the potential flow theory, in which the velocity field is defined by the gradient of a scalar field or velocity potential Φ.

In order to describe the mathematical problem, we consider three sets of right-handed orthogonal coordinate systems as presented next.

1. The first system of coordinates $O-(x, y, z)$ is a right-handed earth-bound axes cartesian system with origin O, with x and y axes in the mean free surface and positive z axis pointing upwards. A point in space has position or displacement vector $\vec{\delta} = (x, y, z)$;
2. The second system $O_g-(X_g, Y_g, Z_g)$ is a right-handed body-bound axes system with origin at the center of gravity of the geosim, with positive X_g axis pointing to the geosim bow direction and the positive Z_g pointing upwards. The hull surface is defined exclusively in this coordinate system, being a point on the geosim surface described by the vector $\vec{r}_g = (X_g, Y_g, Z_g)$. The orientation of a surface element is defined by its normal vector $\vec{n}_g = (n_{gx}, n_{gy}, n_{gz})$, pointing inwards.
3. The third system is equal to the second one, but applied for the barge B. In this way, the index g must be replaced by b.

Accordingly, the geosim body-bound coordinate system is used to describe its oscillatory motions in three degrees of freedom with amplitudes ξ_i, being $i = 1, 3, 5$. Here $i = 1, 3, 5$ represent surge, heave and pitch motions of the geosim, respectively.

The incident wave and the resultant body motions are here assumed to be of small amplitude. In addition, the problem is linearized by expanding the velocity potential and other physical

quantities in power series and by applying the boundary conditions with respect to the mean surface positions.

By following this approach, the total velocity potential Φ is split in a sum of the incident wave velocity potential ϕ_I and the disturbed velocity potential $\phi^{(1)}$, the latter representing both the disturbance of the incident waves diffracted from the bodies and the waves radiated due to the oscillations of the geosim.

The incident regular wave field potential for infinite waters is defined as follows:

$$\phi_I = \frac{A_I g}{\omega} e^{kz} \cos(kx - \omega t) \quad \text{on} \quad z \leq 0, \tag{A.1}$$

which needs to satisfy the wave dispersion relation for infinite water depth:

$$k = \frac{\omega^2}{g}, \tag{A.2}$$

where g, A_I, ω and k are the acceleration gravity, the incident wave amplitude, the wave angular frequency and the wave number, respectively.

Upon these considerations, the well known first order boundary value problem may be summarized as follows:

1. Laplace's equation:

$$\nabla^2 \phi = 0 \quad \text{in fluid domain.} \tag{A.3}$$

2. Kinematic free surface condition:

$$\frac{\partial \phi^{(1)}}{\partial z} = -\frac{\partial \eta^{(1)}}{\partial t} \quad \text{on} \quad z = 0. \tag{A.4}$$

3. Dynamic free surface condition:

$$\eta^{(1)} = -\frac{1}{g}\frac{\partial \phi^{(1)}}{\partial t} \quad \text{on} \quad z = 0. \tag{A.5}$$

4. Bodies boundary conditions:

$$\nabla \phi^{(1)} \cdot \bar{\vec{n}}_g = \frac{\partial \vec{\delta}_g^{(1)}}{\partial t} \cdot \bar{\vec{n}}_g - \nabla \phi_I \cdot \bar{\vec{n}}_g \quad \text{on} \quad \bar{S}_g, \tag{A.6}$$

$$\nabla \phi^{(1)} \cdot \bar{\vec{n}}_b = -\nabla \phi_I \cdot \bar{\vec{n}}_b \quad \text{on} \quad \bar{S}_b. \tag{A.7}$$

5. Far field radiation condition:

$$\nabla \phi^{(1)} \to 0 \quad \text{at} \quad \sqrt{x^2 + y^2 + z^2} \to \infty, \tag{A.8}$$

where $\eta^{(1)}$ is the first order free surface elevation, $\bar{\vec{n}}_{Ag}$ is the geosim zeroth unit order normal vector and $\vec{\delta}_g^{(1)}$ is the time-dependent displacement of the geosim hull, respectively.

In Eq. (A.6), $\bar{\delta}_g$ reads:

$$\vec{\delta}_g^{(1)}(t) = \vec{\xi}_{Tg}^{(1)}(t) + \vec{\xi}_{Rg}^{(1)}(t) \times \bar{\vec{r}}_g, \tag{A.9}$$

in which $\vec{\xi}_{Tg}^{(1)}(t)$ and $\vec{\xi}_{Rg}^{(1)}(t)$ are the translational and rotational motions of the geosim, respectively, and $\bar{\vec{r}}_g$ is the zeroth order position vectors of a point on the body surface relative to its respective body-bound axes coordinate system.

The geosim motions are calculated with the equation of motion presented in (A.10):

$$\boldsymbol{M}_{3\times3}\frac{\partial^2 \vec{\xi}^{(1)}}{\partial t^2} + \boldsymbol{K}_{3\times3}\vec{\xi}^{(1)} = \begin{pmatrix} \vec{F}_g^{(1)} \\ \vec{M}_{g0}^{(1)} \end{pmatrix}, \tag{A.10}$$

where $\boldsymbol{M}$ and $\boldsymbol{K}$ are the inertial and restoring matrices, and the vector $\vec{\xi}^{(1)}$ contains the first order motions for the three degrees of freedom here considered.

In order to conclude this Initial Boundary Value Problem (IBVP), an initial condition must be imposed at the free surface so as to determine the subsequent fluid motions. As demonstrated by [34], for flows beginning from rest we may set the velocity potential at the initial instant $t = 0$ s, to:

$$\Phi = 0 \quad \text{on} \, t = 0\,\text{s}. \tag{A.11}$$

The first order unsteady hydrodynamic pressure, forces and moments on the body hulls are calculated with Eqs. (A.12), (A.13) and (A.14), respectively:

$$p^{(1)} = -\rho\left(\frac{\partial \phi^{(1)}}{\partial t} + \frac{\partial \phi_I}{\partial t}\right), \tag{A.12}$$

$$\vec{F}^{(1)} = \iint_{\bar{S}_B} -\rho\left(\frac{\partial \phi^{(1)}}{\partial t} + \frac{\partial \phi_I}{\partial t}\right)\bar{\vec{n}}\,\mathrm{d}S, \tag{A.13}$$

$$\vec{M}_O^{(1)} = \iint_{\bar{S}_B} -\rho\left(\frac{\partial \phi^{(1)}}{\partial t} + \frac{\partial \phi_I}{\partial t}\right)(\bar{\vec{r}} \times \bar{\vec{n}})\,\mathrm{d}S. \tag{A.14}$$

One should notice that special care must be given to the linear pressure calculation, since there is not an exact equation for the calculation of the potential time-derivative $\partial\phi^{(1)}/\partial t$. In this way, we applied the numerical procedures demonstrated in [32,33], in which the pressure is evaluated directly using the first order acceleration potential (A.15), which also satisfies Laplace's equation in the fluid domain:

$$\Psi^{(1)} = \frac{\partial \phi^{(1)}}{\partial t}. \tag{A.15}$$

By following this method, a second boundary value problem is written for the acceleration potential. The bodies boundary conditions can be defined by derivation in time of the expressions (A.6) and (A.7), as can be seen in (A.16) and (A.17):

$$\nabla \Psi^{(1)} \cdot \bar{\vec{n}}_g = \frac{\partial^2 \vec{\delta}_g^{(1)}}{\partial t^2} \cdot \bar{\vec{n}}_g - \nabla\left(\frac{\partial \phi_I}{\partial t}\right) \cdot \bar{\vec{n}}_g \quad \text{on} \quad \bar{S}_g, \tag{A.16}$$

$$\nabla \Psi^{(1)} \cdot \bar{\vec{n}}_b = -\nabla\left(\frac{\partial \phi_I}{\partial t}\right) \cdot \bar{\vec{n}}_b \quad \text{on} \quad \bar{S}_b. \tag{A.17}$$

In addition, the free surface boundary condition is determined in terms of the dynamic free surface condition for the velocity potential, as presented in (A.18):

$$\Psi^{(1)} = -g\eta^{(1)} \quad \text{on} \quad z = 0. \tag{A.18}$$

The initial condition imposed is presented in (A.19).

$$\Psi^{(1)} = 0 \quad \text{on} \quad t = 0\,\text{s}. \tag{A.19}$$

From now on, the superscript $^{(1)}$ denoting the first order quantities of the formulation will be suppressed in order to simplify the notations.

A.2. Numerical method

In order to solve the initial boundary value problems defined for the velocity and acceleration potentials, the present TDRPM adopts a low order boundary element method using the Rankine's source as Green's function G_{PQ}:

$$G_{PQ} = \frac{1}{\sqrt{(x_p - x_q)^2 + (y_p - y_q)^2 + (z_p - z_q)^2}}, \tag{A.20}$$

where P and Q are field and source points, respectively.

In this method, the integral equations for the velocity and acceleration potentials, presented in Equations (A.21) and (A.22), are solved at a certain time step, whereas a Fourth Order Runge–Kutta Method (RK4) time marching scheme is applied to update the boundary conditions to a new time step.

$$\iint_{\partial\Omega'_{-P}} \left[\phi_Q \frac{\partial G_{PQ}}{\partial n_Q} - G_{PQ}\frac{\partial \phi_Q}{\partial n_Q}\right] \mathrm{d}\partial\Omega' = \begin{cases} -4\pi\phi_P & \text{if } P \text{ inside } \Omega', \\ -2\pi\phi_P & \text{if } P \text{ is at } \partial\Omega', \\ 0 & \text{if } P \text{ is outside } \Omega', \end{cases} \tag{A.21}$$

$$\iint_{\partial\Omega'_{-P}} \left[\Psi_Q \frac{\partial G_{PQ}}{\partial n_Q} - G_{PQ}\frac{\partial \Psi_Q}{\partial n_Q}\right] \mathrm{d}\partial\Omega' = \begin{cases} -4\pi\Psi_P & \text{if } P \text{ inside } \Omega', \\ -2\pi\Psi_P & \text{if } P \text{ is at } \partial\Omega', \\ 0 & \text{if } P \text{ is outside } \Omega'. \end{cases} \tag{A.22}$$

Aiming at guaranteeing a stable evolution of the solution until the achievement of a steady-state, the numerical scheme also considers the use of a ramp function $f_r(t)$ defined by:

$$f_r(t) = \begin{cases} \frac{1}{2}\left[1 - \cos\left(\frac{\pi t}{T_r}\right)\right] & \text{if } t \le T_r, \\ 1 & \text{if } t > T_r. \end{cases} \tag{A.23}$$

where T_r is the ramp time which is set as a multiple of a characteristic wave period involved in the simulations.

Moreover, in order to prevent the diffracted and radiated waves reaching the free surface boundaries and being reflected back to the bodies positions, the numerical damping zone concept, firstly proposed by Israeli and Orszag [35], is imposed near the free surface edge. In fact, this numerical damping zone works similar to the damping lid approach, already discussed, in which a dissipation term is included in the free surface boundary conditions. Among several variations of the method that may be observed in the literature, such as the ones applied in [36–39], in this work the following one [40] has been used:

$$\frac{\partial \eta}{\partial t} = \frac{\partial \phi}{\partial z} - \nu(x,y)\eta \quad \text{at } z = 0 \quad \text{and} \quad \sqrt{x^2+y^2} > L_{dz}, \tag{A.24}$$

$$\frac{\partial \phi}{\partial t} = -g\eta - \nu(x,y)\phi \quad \text{at } z = 0 \quad \text{and} \quad \sqrt{x^2+y^2} > L_{dz}, \tag{A.25}$$

in which L_{dz} is the distance from the global coordinate origin until the begining of the damping region and $\nu(x, y)$ is a function that defines the dissipation characteristic of this region, described by:

$$\nu(x,y) = a\omega\left(\frac{\sqrt{x^2+y^2} - L_{dz}}{b\lambda}\right)^2, \tag{A.26}$$

where a defines the intensity of dissipation and b the damping zone length. These values must be tuned by preliminary tests in order to avoid the occurrence of reflected waves which may spoil the solution. In general, we observe that the damping zone must have a minimum length of one wave length, $b = 1$, whereas the intensity must be set in such a way that permits a progressive and smooth dissipation of the waves. Damping zones with large values of a (i.e $a \ge 3$) may behave as a fixed wall.

References

[1] Zhao WH, Yang JM, Hu ZQ, Wei YF. Recent developments on the hydrodynamics of floating liquid natural gas (FLNG). Ocean Eng 2011;38:1555–67.
[2] Koo B, Kim M. Hydrodynamic interactions and relative motions of two floating platforms with mooring lines in side-by-side offloading operation. Appl Ocean Res 2005;27:292–310.
[3] Kashiwagi M, Endo K, Yamaguchi H. Wave drift forces and moments on two ships arranged side by side in waves. Ocean Eng 2005;32:529–55.
[4] Molin B. On the piston and sloshing modes in moonpools. J Fluid Mech 2001;430:27–50.
[5] Molin B, Remy F, Kimmoun O, Stassen Y. Experimental study on the wave propagation and decay in a channel through a rigid ice-sheet. Appl Ocean Res 2002;24:247–60.
[6] Sun L, Eatock Taylor R, Taylor P. First and second-order analysis of resonant waves between adjacent barges. J Fluid Struct 2010;26:954–78.
[7] Huijsmans RHM, Pinkster JA, de Wilde JJ. Diffraction and radiation of waves around side-by-side moored vessels. In: Proceedings of the 11th ISOPE conference. 2001. p. 406–12.
[8] Hong SY, Kim JH, Cho SK, Choi YR, Kim YS. Numerical and experimental study on hydrodynamic interaction of side-by-side moored multiple vessels. Ocean Eng 2005;32:783–801.
[9] Lewandowski EM. Multi-vessel seakeeping computations with linear potential theory. Ocean Eng 2008;35:1121–31.
[10] Molin B, Remy F, Camhi A, Ledoux A. Experimental and numerical study of the gap resonances in-between two rectangular barges. In: 13th congress of international maritime association of mediterranean IMAM 2009. October 2009.
[11] Kristiansen T, Faltinsen OM. A two-dimensional numerical and experimental study of resonant coupled ship and piston-mode motion. Appl Ocean Res 2010;32:158–76.
[12] Kristiansen T, Faltinsen OM. Gap resonance analyzed by a new domain-decomposition method combining potential and viscous flow draft. Appl Ocean Res 2012;34:198–208.
[13] Elie B, Reliquet GP-EG, Thilleul O, Ferrant P, Gentaz L, Ledoux A. Simulation of the gap resonance between two rectangular barges in regular waves by a free surface viscous flow solver. In: Proceedings of the ASME 2013 32nd international conference on ocean, offshore and artic engineering, OMAE2013. 2013.
[14] Newman JN. Application of generalized modes for the simulation of free surface patches in multi body hydrodynamics. Tech. rep., Wamit Consortium Report; 2003.
[15] Chen C-B. Hydrodynamic analysis for offshore LNG terminals. In: Proceedings of the 15th ISOPE conference. 2005.
[16] Fournier JR, Naciri M, Chen XB. Hydrodynamics of two side-by-side vessels. experiments and numerical simulations. In: Proceedings of the 16th ISOPE conference. 2006.
[17] Pauw WH, Huijsmans RHM, Voogt A. Advances in the hydrodynamics of side-by-side moored vessels. In: Proceedings of the 26th international conference on offshore mechanics and artic engineering, OMAE 2007. 2007.
[18] Bunnik T, Pauw W, Voogt A. Hydrodynamic analysis for side-by-side offloading. In: Proceedings of the 19th ISOPE conference. 2009.
[19] Hong DC, Hong SY, Nam BW, Hong SW. Comparative numerical study of repulsive drift forces and gap resonances between two vessels floating side-by-side in proximity in head seas using a discontinuous HOBEM and a constant BEM with boundary matching formulation. Ocean Eng 2013;72:331–43.
[20] Clauss GF, Dudek M, Testa D. Gap effects at side-by-side LNG-transfer operations. In: OMAE 2013-10749, Proceedings of the 32nd international conference on ocean, offshore and arctic engineering. 2013.
[21] Buchner B, Van Dijk A, de Wilde JJ. Numerical multiple-body simulations of side-by-side mooring to a FPSO. In: Proceedings of the 21st ISOPE conference. 2001. p. 343–53.
[22] Naciri M, Waals O, de Wilde J. Time domain simulations of side-by-side moored vessels lessons learnt from a benchmark test. In: Proceedings of the OMAE2007 26th international conference on offshore mechanics and artic engineering. 2007.
[23] Zhao W, Yang J, Hu Z, Tao L. Prediction of hydrodynamic performance of an flng system in side-by-side offloading operation. J Fluid Struct 2013;46:89–110.
[24] Cummins W. The impulsive response function and ship motions. Tech. rep. Department of the Navy David Taylor Model Basin; 1962.
[25] Kim K-H, Kim Y. Time-domain analysis of motion responses of adjacent multiple floating bodies in waves. In: Proceedings of the 18th ISOPE conference. 2008.
[26] Yan S, Ma QW, Cheng X. Fully nonlinear hydrodynamic interaction between two 3d floating structures in close proximity. In: Proceedings of the 19th ISOPE conference. 2009.
[27] Hong SY, Nam B. Analysis of 2nd-order wave force on floating bodies using fem in time domain. Int J Offshore Polar Eng 2011;21:22–8.
[28] Watai RA, Ruggeri F, Sampaio CMP, Simos AN. Development of a time domain boundary elements method for numerical analysis of floating-bodies responses in waves. J Braz Soc Mech Sci Eng 2014 (Under revision).
[29] WAMIT. WAMIT 7.0 user manual. The Massachusets Institute of Technology; 2012.
[30] Tannuri EA, Bravin TT, Simos AN, Alves KH, Nishimoto K, Ferreira MD. Dynamic simulation of offloading operation considering wave interactions between vessels. In: Proceedings of OMAE04 23nd international conference on offshore mechanics and artic engineering. 2004.
[31] Bunnik T. A simulation approach for large relative motions of multi-body offshore operations in waves. In: Proceedings of the ASME 2014 33rd international conference on ocean, offshore and arctic engineering, OMAE2014. 2014.
[32] van Daalen EFG. Numerical and theoretical studies of water waves and floating bodies. University of Twente; 1993 (PhD thesis).
[33] Tanizawa K. A nonlinear simulation method of 3-d body motions in waves. In: 10th workshop on water waves and floating bodies. 1995. p. 235–9.
[34] Stoker JJ. Water waves. New York, N.Y. Interscience Publishers; 1957.
[35] Israeli M, Orszag SA. Approximation of radiation boundary conditions. J Comput Phys 1981;41:115–35.

[36] Prins H. Time-domain calculations of drift forces and moments. Tecnische Universiteit Delft; 1995 (PhD thesis).
[37] Bunnik THJ. Seakeeping calculations for ships, taking into account the nonlinear steady waves. Technische Universiteit Delft; 1999 (PhD thesis).
[38] Boo SY. Linear and nonlinear irregular waves and forces in a numerical wave tank. Ocean Eng 2002;29:475–93.
[39] Shao Y-L. Numerical potential-flow studies on weakly-nonlinear wave-body interactions with/without small forward speeds. Norwegian University of Science and Technology; 2010 (PhD thesis).
[40] Zhen L, Bin T, De-zhi N, Ying G. Wave–current interactions with three-dimensional floating bodies. J Hydrodyn 2010;22:229–40.